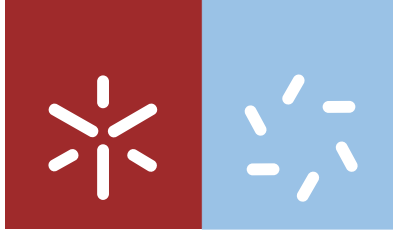


Universidade do Minho
Escola de Ciências

Ana Marina Araújo Amorim

**Neuropathologic study of a transgenic mouse
model of Machado-Joseph disease**



Universidade do Minho

Escola de Ciências

Ana Marina Araújo Amorim

**Neuropathologic study of a transgenic mouse
model of Machado-Joseph disease**

Dissertação de Mestrado
Mestrado em Genética Molecular

Trabalho realizado sob a orientação da
Professora Doutora Patrícia Maciel
e co-orientação da
Professora Doutora Maria João Sousa
e da
Doutora Anabela Silva-Fernandes

outubro de 2013

DECLARAÇÃO

Nome: Ana Marina Araújo Amorim

Endereço electrónico: a.marinaamorim@gmail.com

Número de identificação civil: 13786636

Título da dissertação de mestrado: Neuropathologic study of a transgenic mouse model of Machado-Joseph disease.

Orientador: Professora Doutora Patrícia Maciel

Co-orientadores: Professora Doutora Maria João Sousa e Doutora Anabela Silva-Fernandes.

Ano de conclusão: 2013

Designação do Mestrado: Genética Molecular

É AUTORIZADA A REPRODUÇÃO INTEGRAL DESTA DISSERTAÇÃO APENAS PARA EFEITOS DE INVESTIGAÇÃO, MEDIANTE DECLARAÇÃO ESCRITA DO INTERESSADO, QUE A TAL SE COMPROMETE.

Universidade do Minho, 31 de Outubro de 2013.

Assinatura: _____

AGRADECIMENTOS

Gostaria de agradecer a todas as pessoas que contribuíram para a realização desta tese.

Um agradecimento muito especial à Professora Patrícia Maciel por tão bem me ter recebido no grupo da Machado-Joseph e por sempre se ter demonstrado carinhosa, entusiasmada com o meu trabalho e por ter sido extremamente delicada e compreensiva comigo durante todo o meu percurso no ICVS.

Aproveito também para agradecer à Professora Maria João Sousa pela disponibilidade e pela preocupação que teve comigo desde o início deste projeto.

À Anabela por me ter ensinado tudo! Por ser uma orientadora no laboratório, no microscópio, no biotério....E por ser uma pessoa amável, muito simpática e amiga.

À Sara por ser uma pessoa por quem eu tenho um carinho muito especial e por ser a menina mais prestável que conheci no ICVS no sentido em que está sempre disposta a ajudar mesmo que esteja “atulhada” de trabalho. Obrigada pelas vezes em que me disseste: “Marina, que precisas? Achas que eu posso ajudar?” Obrigada até pelos momentos em que dizias: “Se alguém te ralhar, tu diz-me! Que eu digo para te fazerem pior!” ☺

À Sofia Esteves por me ter proporcionado momentos de puro riso. Pelas manhãs animadas passadas no Rotarod e por me elucidar acerca do meu dom para marcação de tubos de sacrifício...

À Cristina Mota por ser minha amiga e companheira de microscópio. Por me tirar imensas dúvidas de estereologia e por ser tão correta naquilo que faz!

Quero agradecer ao Professor Nuno Sousa por me ter aceite no domínio das Neurociências, apesar de não ser aluna de Mestrado Ciências da Saúde. A todos os restantes NeRD que tão bem me receberam e com quem, em alguns casos, construí verdadeiras amizades...

Finalmente, o meu mais especial Obrigada: Aos meus pais, à minha família a quem devo tudo o que sou! À minha irmãzinha mais especial do mundo Driquinhas, à minha prima Leonor que é irmã/amiga/tudo para mim! E às minhas meninas amigas e eternas companheiras para a vida Ru, Ana e Marisa.

ABSTRACT

“Neuropathologic study of a transgenic mouse model of Machado-Joseph disease”

Machado-Joseph Disease (MJD) is an autosomal dominant neurodegenerative disorder caused by an expansion of the polyglutamine tract near the C-terminus of the *ATXN3* gene product, ataxin-3 protein. Clinically, MJD is a very heterogeneous disorder, being the most common symptoms ataxia, loss of balance and coordination, and spasticity. The mutant ataxin-3 forms intranuclear and axonal aggregates in the brain cells of MJD patients. The remarkable degree of brain atrophy observed *post-mortem* in brains of patients with this disorder as well as in other polyQ diseases would suggest that neuronal cell loss is a major feature of the pathogenic process. In order to understand if and how the expanded form of the gene causes cell demise in specific populations of neurons we performed stereological analysis, in order to determine the volumes and the number of cells in specific brain regions (known to be affected in MJD patients) in a transgenic mouse model of the disease. CMVMJD135 mice express ataxin-3 with 135 glutamines under the control of the CMV (cytomegalovirus) promoter and manifest MJD-like motor symptoms including balance deficit, gait ataxia and motor uncoordination that gradually appear and progress overtime, in the absence of premature death. They also show ataxin-3-positive intranuclear inclusions in several brain regions, namely in the pontine and dentate nuclei.

We found a decrease in the volume and total cell number in pontine nuclei and reduction of volume in dentate nuclei, with no differences in the total cell number. No differences were found in volume and total cell number in locus coeruleus and in substantia nigra; however, we observed a decrease of the number of dopaminergic neurons in substantia nigra *pars compacta*. In the cerebellum, we observed a reduction of molecular layer thickness. All together, these findings allow us to conclude that CMVMJD135 mouse is a promising model to study neurodegeneration in MJD, as it reproduces the specific neuronal loss observed in patients in a late stage of the disease. With this work we have identified possible quantitative biomarkers that could be very usefull in future pre-clinical trials with this model.

RESUMO

“Estudo neuropatológico num modelo de ratinho transgénico da doença de Machado- Joseph”

A Doença de Machado-Joseph (DMJ) é uma doença neurodegenerativa autossómica dominante causada por uma expansão anormal de repetições do trinucleótido CAG no gene *ATXN3*. Clinicamente, a DMJ é bastante heterogénea, constituindo os sintomas mais comuns a ataxia, perda de equilíbrio e de coordenação e espasticidade. A ataxina-3 expandida forma agregados intranucleares e axonais nos neurónios de doentes de Machado-Joseph. A atrofia observada em cérebros de pacientes *post-mortem*, bem como em outras doenças provocadas por expansão de glutaminas, sugere como característica chave do processo patogénico a morte neuronal. De modo a compreender como a forma expandida da proteína ataxina-3 afeta determinadas populações neuronais, foi realizada uma análise estereológica, de modo a determinar o volume e número total de células em regiões específicas do cérebro, descritas como afetadas na DMJ, num modelo da doença em ratinho. O ratinho transgénico CMVMJD135 expressa a proteína ataxina-3 com 135 glutaminas sob o controlo do promotor CMV (citomegalovirus) e manifesta sintomas motores característicos da DMJ que incluem perda de equilíbrio, ataxia e falta de coordenação motora que gradualmente progridem ao longo do tempo, na ausência de morte prematura. Apresenta ainda inclusões intranucleares de ataxina-3 em várias regiões do cérebro, tais como núcleos pânticos e denteados. Os resultados deste trabalho mostram uma redução do volume e do número total de células nos núcleos pânticos e uma redução do volume dos núcleos denteados que não é acompanhada por redução do número total de células. Não foram encontradas diferenças no volume e no número de total de células no locus coeruleus e na substância nigra; no entanto, observamos uma diminuição do número de neurónios dopaminérgicos na substância nigra *pars compacta*. Também verificámos uma redução da espessura da camada molecular do cerebelo. Em conjunto, estas descobertas permitem-nos concluir que o ratinho transgénico CMVMJD135 é um modelo promissor para estudar o processo de neurodegeneração na DMJ uma vez que ele reproduz a perda neuronal específica observada em doentes de Machado-Joseph. As alterações aqui identificadas constituem ainda biomarcadores possíveis de quantificação, de grande utilidade em futuros ensaios pré-clínicos usando este modelo animal.

INDEX

DECLARAÇÃO	ii
AGRADECIMENTOS	iii
ABSTRACT	v
RESUMO	vii
INDEX	ix
ABBREVIATIONS	xi
LIST OF FIGURES	xiii
LIST OF TABLES	xv
1. INTRODUCTION	1
1.1. Polyglutamine diseases – Overview.....	3
1.2. MJD – Machado-Joseph disease	6
1.2.1. Epidemiology and Clinical features.....	7
1.2.2. Neuropathology.....	8
1.2.3. Cell death.....	11
- In MJD patients.....	11
- In mouse models of MJD.....	12
1.2.4. Genetics.....	14
1.2.5. Ataxin-3.....	15
1.2.6. Mouse models.....	16
1.2.7. A new mouse model: CVMMJD135.....	20
2. OBJECTIVES	23
3. MATERIAL AND METHODS	27
3.1. Animals.....	29
3.2. DNA extraction and mouse genotyping.....	29
3.3. Molecular analysis of the (CAG) _n repeat.....	30

3.4. Stereology.....	30
3.4.1. Tissue preparation and staining.....	30
3.4.2. Design-based stereology.....	31
3.4.3. Cavalieri’s principle: volume estimation.....	31
3.4.4. Fractionator: neuronal number estimation.....	32
3.5. Immunohistochemistry.....	34
3.6. Estimation of cerebellar layer thickness.....	35
3.7. Statistical analysis.....	36
4. RESULTS	37
4.1. Quantification of volume and total number of cells in brain regions known to be affected in MJD.....	39
4.1.1. Pontine nucleus.....	39
4.1.2. Locus coeruleus.....	41
4.1.3. Substantia nigra.....	43
4.1.4. Dentate nucleus.....	45
4.2. Quantification of specific cell types – neurons and astrocytes – in CMVMJD135 mouse brains.....	48
4.2.1. Quantification of dopaminergic neurons in substantia nigra.....	51
4.3. Analysis of cerebellar layer thickness in CMVMJD135.....	54
5. DISCUSSION	57
6. CONCLUSIONS	63
7. FUTURE PERSPECTIVES	67
8. REFERENCES	71

ABBREVIATIONS

AD – Autosomal dominant

AR – Androgen receptor gene

Asf – Area sampling fraction

ATN1 – Atrophin-1 gene

ATX1 – Ataxin-1 gene

ATX2 – Ataxin-2 gene

ATXN3 - Ataxin-3 gene

CACNA1A - Calcium channel, voltage-dependent, P/Q type, alpha 1A subunit gene

cDNA – Complementary deoxyribonucleic acid

CMV- Cytomegalovirus

CNS – Central nervous system

DAB – 3,3-Diaminobenzidine

DAT – Dopamine transporter

dH₂O – Distilled water

DMJ – Doença de Machado-Joseph

DN – Dentate nuclei

DNA – Deoxyribonucleic acid

DRPLA – Dentatorubral-pallidoluysian atrophy

FELASA – Federation for laboratory animal science associations

GFAP – Glial fibrillary acidic protein

H&E – Hematoxylin and eosin

HD – Huntington's disease

HTT – Huntingtin gene

IF – Intermediate filament

IHC – Immunohistochemistry

kDA – KiloDalton

LC – Locus coeruleus

LC-NA – Locus coeruleus – noradrenergic system

L-DOPA – L-3,4-dihydroxyphenylalanine

MJD – Machado-Joseph disease

MRI – Magnetic resonance imaging

mRNA – Messenger ribonucleic acid
NAT – Noradrenalin transporter
NES – Nuclear export signal
NET – Norepinephrine transporter
NeuN – Neuronal nuclei
NLS – Nuclear localization signal
NNIs – Neuronal nuclear inclusion bodies
PBS – Phosphate buffered saline
PCR – Polymerase chain reaction
PCUF – Preculminate fissure
PFA – Paraformaldehyde
PN – Pontine nuclei
PolyQ – Polyglutamine diseases
SBMA – Spinal bulbar muscular atrophy
SCA – Spinocerebellar ataxia
SF – Secondary fissure
SN – Substantia nigra
Ssf – Section sampling fraction
TBP – TATA box binding protein gene
TH – Tyrosine hydroxylase
TUNEL – Terminal deoxynucleotidyl-transferase (TdT)-mediated *in situ* nick end labelling
UPS – Ubiquitin proteasome pathway
UTR – Untranslated region
XR – X- linked recessive
YAC – Yeast artificial chromosome

LIST OF FIGURES

Figure 1. Sagittal T1-weighted images of the brainstem and cerebellum in patients with SCA3 and in a healthy control subject.....	9
Figure 2. Representation of <i>ATXN3</i> gene structure.....	15
Figure 3. Summary of behaviour and pathology findings in CMVMJD135.....	21
Figure 4. Formula of estimation of the total number of cells.....	32
Figure 5. Counting frame of the optical dissector.....	33
Figure 6. Measurements of molecular and granular layers of cerebellum in secondary fissure.....	36
Figure 7. Illustration of cortico-pontine (PN)-cerebellar pathway.....	40
Figure 8. Low magnification micrograph of glycolmethacrylate-embedded coronal section of pontine nuclei of the mouse stained with Giemsa and the corresponding atlas scheme used for delineation of the region.....	40
Figure 9. Total volume and total number of cells of pontine nuclei calculated for wild-type and CMVMJD135 mice.....	41
Figure 10. Illustration of the locus coeruleus (LC) – noradrenergic system.....	42
Figure 11. Low magnification micrograph of glycolmethacrylate-embedded coronal section of locus coeruleus of mouse stained with Giemsa and the corresponding atlas scheme used for delineation of the region.....	42
Figure 12. Total volume and total number of cells of locus coeruleus calculated for wild-type and CMVMJD135 mice.....	43
Figure 13. Illustration of the major basal ganglia loop.....	44

Figure 14. Low magnification micrographs of glycolmethacrylate-embedded coronal section of substantia nigra of the mouse stained with Giemsa and the corresponding atlas scheme used for delineation of the region.....	44
Figure 15. Total volume and total number of cells of substantia nigra calculated for wild-type and CMVMJD135 mice.....	45
Figure 16. Illustration of the dentato(rubro)thalamocortical pathway.....	46
Figure 17. Low magnification micrographs of glycolmethacrylate-embedded coronal section of dentate nuclei of the mouse stained with Giemsa and the corresponding atlas scheme used for delineation of the region.....	46
Figure 18. Total volume and total number of cells of dentate nuclei calculated for wild-type and CMVMJD135 mice.....	47
Figure 19. GFAP immunostaining of the pontine nuclei in CMVMJD135 and wild-type animals at late stage of the disease and the quantification of the number of GFAP-positive cells calculated for wild-type and CMVMJD135 mice in pontine nuclei.....	49
Figure 20. NeuN immunostaining of the pontine nuclei in CMVMJD135 and wild-type animals at late stage of the disease and the quantification of the number of NeuN-positive cells calculated for wild-type and CMVMJD135 mice in pontine nuclei.....	50
Figure 21. Tyrosine-hydroxylase immunostaining in substantia nigra in CMVMJD135 and wild-type animals at late stage of the disease.....	52
Figure 22. Number of TH-positive cells calculated for wild-type and CMVMJD135 mice in substantia nigra.....	53
Figure 23. Low magnification micrograph of a sagittal section of cerebellum of the mouse stained with hematoxylin and the corresponding atlas scheme used for the identification of the preculminate fissure and secondary fissure.....	55
Figure 24. Measurements of molecular and granular layers of cerebellum calculated for wild-type and CMVMJD135 mice.....	55

LIST OF TABLES

Table 1. Pathogenic features of polyglutamine diseases.....	4
Table 2. Clinical features of polyglutamine diseases.....	5
Table 3. Mean cross sectional area (upper spinal cord) in SCA3 and controls.....	9
Table 4. Summary of the CNS components that undergo neurodegeneration during the course of MJD.....	10
Table 5. Neuronal loss observed in MJD mouse models.....	13
Table 6. Brain Pathology of the Mouse Models for MJD.....	19

1. INTRODUCTION

1.1. Polyglutamine diseases - Overview

Polyglutamine diseases (PolyQ) are a large group of inherited neurodegenerative conditions. They are characterized by the pathologic expansion of CAG trinucleotide repeats in translated sequences of distinct genes (Bauer and Nukina, 2009). Currently, nine polyQ-related disorders are known: spinal bulbar muscular atrophy (SBMA), Huntington's disease (HD), dentatorubral-pallidoluysian atrophy (DRPLA), and six types of spinocerebellar ataxias (SCA1, 2, 3, 6, 7 and 17) (Zoghbi and Orr, 2000). They have different incidence rates, HD and SCA3, also known as Machado Joseph disease, being the most common (Schöls et al, 2004).

The CAG expansion leads to an abnormally long polyglutamine tract within proteins involved in the disease. A common feature of all polyQ disorders is the accumulation of mutant protein in the neuronal cells causing their dysfunction and eventually death (Bauer and Nukina, 2009). As represented in Table 1, for each polyQ disorder the subcellular localization of the aggregates in neurons can vary among nuclear and cytoplasmic inclusions. The number of CAG repeats in neurons can also vary. The expanded, longer than normal, polyglutamine repeats are unstable and tend to expand further in next generations. This leads to earlier age at onset and a more severe phenotype in successive generations - a phenomenon known as anticipation (Schöls et al, 2004).

Studies have investigated which structure of expanded polyglutamine is responsible for disease progression. The hypothesis that a toxic structure of expanded polyglutamine causes the disease explains its length-dependence and implies a common mechanism of pathogenesis in polyQ diseases, however it is not sufficient to explain the selective pattern of toxicity of these causative proteins that leads to different neuropathologic involvement and clinical manifestations (Takahashi et al, 2010).

Table 1. Pathogenic features of polyglutamine diseases (adapted from Ross, 1995; Seidel et al, 2012).

Disease	Causative gene	CAG repeat size		Aggregates	Brain regions atrophy
		Normal	Disease		
HD	<i>HTT</i>	6 to 35	36 to 121	Cytoplasmic	Striatum and cerebrum cortex
DRPLA	<i>ATN1</i>	3 to 38	49 to 88	Cytoplasmic	Pallidum, subthalamic, dentate nuclei and red nucleus
SBMA	<i>AR</i>	6 to 36	38 to 62	Nuclear and cytoplasmic	Anterior horn, bulbar neurons and dorsal route ganglia
SCA1	<i>ATX1</i>	6 to 39	41 to 83	Nuclear	Cerebellum and brainstem
SCA2	<i>ATX2</i>	14 to 32	34 to 77	Nuclear and cytoplasmic	Cerebellum, pons, medulla oblongata and spinal cord
SCA3/MJD	<i>ATXN3</i>	12 to 40	62 to 86	Nuclear and cytoplasmic	Cerebellum, brainstem and spinal cord
SCA6	<i>CACNA1A</i>	4 to 18	21 to 30	Cytoplasmic	Cerebellum and brainstem
SCA7	<i>SCA7</i>	7 to 18	38 to 200	Nuclear	Cerebellum and brainstem
SCA17	<i>TBP</i>	25 to 43	45 to 63	Nuclear	Cerebrum, cerebellum and brainstem

In spite of these commonalities, in most cases, the neuropathology of each polyQ disease is associated with a specific subset of neurons. However, it is not clear the relationship between expression pattern and pathology location, once the causative proteins are widely expressed in the Central Nervous System (CNS) as well as in peripheral tissues (Gusella and MacDonald, 2000), except for SCA6, where the gene product is expressed predominantly in Purkinje cells of the cerebellum (highly affected in SCA6) (Ishikawa et al, 1999) and in SBMA, where the androgen receptor is primarily expressed in the vulnerable motor neurons (reviewed in Costa and Paulson, 2012).

All of these polyQ disorders are dominantly inherited in an autosomal manner with the exception of SBMA, which is X-linked and was the first disease connected with the expansion of CAG repeat causing progressive motor neuron degeneration (La Spada et al, 1991). Specific affected neuronal populations are still an important object

of study in these disorders because they differ among diseases and determine the characteristic clinical symptoms associated with each disorder. For instance, HD patients show neurodegeneration in the striatum leading to uncontrolled movements whereas in SCA_s cell loss occurs mainly in the cerebellum, causing ataxia (table 2).

Table 2. Clinical features of polyglutamine diseases (adapted from Takahashi et al, 2010).

Disease	Inheritance	Clinical features
SBMA	XR	Weakness, bulbar symptom, fasciculations, tremors, gynecomastia.
HD	AD	Chorea, dystonia, dementia.
DRPLA	AD	Myoclonus epilepsy, ataxia, chorea, dementia.
SCA1	AD	Ataxia, bulbar symptom, spasticity, polyneuropathy, cognitive impairment.
SCA2	AD	Ataxia, slow saccades, ataxia, polyneuropathy, parkinsonism.
SCA3	AD	Ataxia, spasticity, polyneuropathy, diplopia, dystonia.
SCA6	AD	Ataxia, dysarthria, down-beating nystagmus.
SCA7	AD	Ataxia, retinal degeneration, ophthalmoplegia.
SCA17	AD	Ataxia, dementia, psychosis, seizures, extrapyramidal signs.

XR, X-linked recessive; AD, autosomal dominant.

The role of the aggregation in disease pathogenesis is not clear. It is controversial whether the toxicity of the expanded polyQ proteins results from the presence of visible aggregates or from smaller intermediary species generated during the aggregation process. Aggregates may just represent end products of the upstream toxic event (Bauer and Nukina, 2009). Some studies have suggested that the inclusions have a protective role (Saudou et al, 1998). Several issues have been studied regarding pathogenesis of polyglutamines: i) whether the specific structure of expanded polyglutamine results in toxicity to cells; ii) the type of dysfunction that leads to disease as well as iii) how the expanded polyglutamine protein causes dysfunction (Takahashi et al, 2010).

Until now, there is no effective therapy preventing the physical (and in some polyQ diseases also mental) decline caused by the dysfunction and eventually death of neurons in these disorders, aggravated by the accumulation of mutant proteins inside neurons (Bauer and Nukina, 2009).

1.2. MJD – Machado-Joseph disease

Machado-Joseph disease was first studied in 1972 by Nakano and co-workers. They characterized this disease as a hereditary ataxia in Portuguese emigrants to Massachusetts. They studied the first family affected by a progressive cerebellar degeneration transmitted in autosomal dominant manner and named this disorder as Machado disease (Nakano et al, 1972). In the same year, Woods and Schaumburg reported a study in other family, also from Azores Islands and established in Massachusetts, that presented similar clinical symptoms; They characterized the disease as an autosomic dominant disorder, however they named it as “nigrospinodontal degeneration with nuclear ophthalmoplegia” (Woods and Schaumburg, 1972). In 1976, a separate entity was reported in an Azorean family, the Joseph family, emigrated to California; Researchers classified the disorder as an autosomal dominant striatonigral degeneration and called it as “Joseph disease” (Rosenberg et al, 1976). One year later, the fourth family was studied and the disease was this time described as “Azorean disease of the nervous system” (Romanul et al, 1977). In 1978, Coutinho and Andrade studied 40 patients from 15 families affected by an autosomal dominant late onset genetic disorder from the Azorean Islands and reported that this genetic disease had variable phenotypic patterns, which were variations of the same disorder, proposing the name of Machado-Joseph disease. They classified the clinical features of the disease in three main types in order to comprise the different patterns of neuropathology observed until then in MJD patients (Coutinho and Andrade, 1978).

Presently, MJD, also called spinocerebellar ataxia type 3 (SCA3), is known to be the most common dominantly inherited ataxia worldwide (15- 45% of all forms in different countries and ethnic populations) (Paulson, 2007).

MJD is caused by the expansion of CAG repeat in the *ATXN3* gene causing an extension of a polyglutamine repeat in the C-terminus of the gene protein product ataxin-3 (Kawaguchi et al, 1994). In normal individuals ataxin-3 contains between 12 and 40 glutamines, whereas most of the clinically diagnosed MJD patients show expansion of the repeat-number from 60 to 84 (Paulson et al, 2000).

CAG expansion has a dynamic behaviour, which reflects on the general tendency of expanded repeats to become larger when transmitted to next generation. Nevertheless, there is a differential instability of the CAG tract length between male and female transmissions. Repeat instability appears to be more frequent when transmission

occurs through a male than through a female (Maciel et al, 1995). This dynamic feature of the disease mutation explains the phenomenon of anticipation observed in some MJD families, in which affected offspring tend to manifest disease earlier than an affected parent (Sequeiros and Coutinho, 1993). In MJD, CAG repeat instability can also occur in different cells from the same tissue, a phenomenon known as somatic mosaicism (Maciel et al, 1997).

1.2.1. Epidemiology and Clinical features

MJD is presently considered the most common form of SCA worldwide, with families described in Portugal, Spain, Singapore, the Netherlands, Germany, Italy, the Czech Republic, United States, Canada, Brazil, Mexico, China, Japan, India and Australia. The relative frequency of MJD is higher in countries such as Brazil (69-92%) and Portugal (58-74%) with high prevalence in the Azores Islands, namely Flores Island (1/239) (Bettencourt and Lima, 2011). In contrast, MJD is almost absent in Italy and in the Czech Republic (Bauer and Nukina, 2009).

MJD symptoms begin to manifest by the age of 30-50 years, usually culminating in early death (on average 20 years after the onset of disease). The symptoms of this polyQ disorder comprise cerebellar ataxia, peripheral nerve palsy, pyramidal and extrapyramidal features (Rosenberg, 1992). There are other specific characteristics that can be of major importance for the clinical diagnosis of MJD such as external progressive ophthalmoplegia, dystonia, intention fasciculation-like movements of facial and lingual muscles, as well as lid retraction, originating the aspect of “bulging eyes”. MJD encompasses a wide high clinical spectrum and it can be divided in four different phenotypes: type I corresponds to an early onset (10 to 30 years) which is characterized by extrapyramidal (mainly dystonic) and pyramidal deficits; type II has an intermediate onset, it appears between 20 and 50 years and is marked by pyramidal and cerebellar deficits; type III is featured by a late onset (40 to 75 years) emerging with cerebellar deficits and peripheral neuropathy (Coutinho and Andrade, 1978). Finally, type IV is the rarest and is characterized by uncertain onset, arising with neuropathy and parkinsonism (Rosenberg, 1992).

Although no cure or treatment for this disease has been discovered yet, symptomatic treatment can relieve some symptoms caused by the disease. Spasticity can be efficiently treated with baclofen, tizanidine or memantine combined with

dopaminergic treatment (Riess et al, 2008). Amantadine and small dosages of botulinum toxin can be beneficial for dystonia (Woods and Schaumburg, 1972) and muscle cramps can be ameliorated with magnesium, mexiletine and chinine (Kanai et al, 2003). Dopaminergic treatment is the long lasting therapy for Parkinsonism symptoms (Buhmann et al, 2003). Besides, daily training of gait and physiotherapy can also help to meliorate ataxia symptoms. Logopedic treatment is good for dysarthria and dysphagia in order to maintain the ability to communicate and to prevent pneumonia from aspiration. Nevertheless, the efficacy of these approaches decreases with time and eventually the disease progression is unavoidable (Riess et al, 2008).

1.2.2. Neuropathology

MJD affects a large variety of functional and neurotransmitter systems and it results in a central nervous distribution pattern of lesions that is widespread and severe (Seidel et al, 2012).

Magnetic resonance spectroscopy analysis of deep white matter has shown metabolic abnormalities suggestive of axonal dysfunction in MJD patients (D'Abreu et al, 2009). Positron emission tomography studies on the regional cerebral glucose metabolism revealed a significantly decreased glucose utilization in the cerebellum, brainstem, striatum and whole cerebral cortex (Taniwaki et al, 1997). Moreover, decreased binding for DAT (Dopamine transporter) in these regions was observed in symptomatic MJD patients (Wüllner et al, 2005).

Enlargement of the fourth ventricle is the most consistent feature observed by magnetic resonance imaging (MRI) in MJD patients. Furthermore, the neuropathology of MJD includes severe neuronal loss in the anterior horn and Clarke's column of the spinal cord (table 3) and in restricted brain regions such as dentate nucleus (cerebellum), pontine nuclei and locus coeruleus (brainstem), substantia nigra (basal ganglia) and other regions such as the thalamus, as well as subthalamic, red and cranial nerve nuclei (Romanul et al, 1977). It is also characterized by axonal neuropathy of peripheral motor and sensory axons (Klockgether et al, 1999).

Table 3. Mean cross sectional area (upper spinal cord) in SCA3 and controls
(adapted from Lukas et al, 2008).

Type	Mean cross-sectional area (mm ²)	p-value
SCA3	59.02 ± 8.5	< 0.0005
Control group	82.17 ± 8.4	

In MJD, the atrophy in the cerebellum and brainstem (figure 1) is progressive and dependent on the length of the CAG repeat and the age of the patients (Eichler et al, 2011). However, different brain regions present different rates of atrophy and progression. While atrophy of the cerebellum and pontine base seem to correlate with patient's age, atrophy of the midbrain and pontine tegmentum show no significant progression in longitudinal studies by MRI with observation periods of 4.5–10.6 years, compatible with very slow evolution of pathology in these regions (Horimoto et al, 2008).

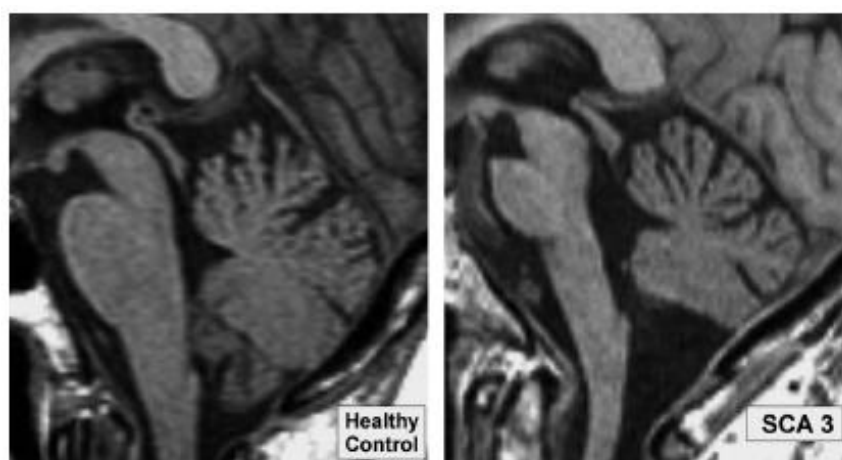


Figure 1. Sagittal T1-weighted images of the brainstem and cerebellum in patients with SCA3 and in a healthy control subject (adapted from Eichler et al, 2011).

Upon macroscopic examination, the brains of MJD patients with a disease duration of more than 15 years showed a depigmentation of the substantia nigra, a considerable atrophy of the cerebellum, pons, and medulla oblongata; an atrophy of the cranial nerves III to XII were also consistently observed (Rüb et al, 2008). In addition, in the majority of these MJD patients, the total brain weight was lower than that of

individuals without medical histories of neurological or psychiatric diseases, which by itself is an indicator of brain atrophy in patients (Bürk et al, 1996). In contrast to previous conventional neuropathological studies, recent pathoanatomical studies involving unconventional serial thick tissue sections demonstrated a more extensive damage affecting areas of the cerebellothalamocortical motor loop, the basal ganglia-thalamocortical motor loop, and several other systems: visual, auditory, somatosensory, vestibular, oculomotor, ingestion-related brainstem nuclei, precerebellar brainstem, cholinergic and dopaminergic midbrain, and pontine noradrenergic systems (table 4) (Rüb et al, 2008).

Table 4. Summary of the CNS components that undergo neurodegeneration during the course of MJD (Rüb et al, 2008).

Affected central nervous component	Major lesions
Cerebellothalamocortical motor loop	Cerebellar cortex, dentate and fastigial nuclei; pontine nuclei; thalamic ventral lateral nucleus; giant Betz pyramidal cells of the primary motor cortex; anterior horn motoneurons of the spinal cord
Basal ganglia–thalamocortical motor loop	Pallidum; subthalamic nucleus; thalamic ventral lateral and reticular nuclei
Visual system	Lateral and inferior nuclei of the pulvinar; lateral geniculate body of the thalamus
Auditory system	Inferior colliculus; nuclei of the lateral lemniscus; superior olive; cochlear nuclei
Somatosensory system	All somatosensory nuclei of the thalamus, pons and medulla oblongata; Clarke’s column of the spinal cord
Vestibular system	Superior, lateral, medial, spinal and interstitial vestibular nuclei
Oculomotor system	Oculomotor, trochlear, and abducens nuclei; rostral interstitial nucleus of the medial longitudinal fascicle; reticulotegmental nucleus of the pons; area of the excitatory burst neurons for horizontal saccades; raphe interpositus nucleus; prepositus hypoglossal nucleus
Ingestion-related brainstem system	All somatosensory, somatomotor, viscerosensory and visceromotor ingestion-related brainstem nuclei; ingestion-related regions of the brainstem reticular formation
Precerebellar brainstem system	Arcuate nucleus; red nucleus; pontine nuclei; reticulotegmental nucleus of the pons; vestibular nuclei; lateral reticular nucleus; external cuneate nucleus; prepositus hypoglossal nucleus; dorsal paramedian reticular nucleus; nucleus Roller; inferior olive
Midbrain dopaminergic system	Mesostriatal dopaminergic system (substantia nigra); mesolimbic dopaminergic system (nuclei of the ventral tegmental area)
Midbrain cholinergic system	Pedunculo-pontine nucleus
Pontine noradrenergic system	Locus coeruleus

Furthermore, these recent studies revealing that the widespread damage of cerebellum, thalamus, midbrain, pons, medulla oblongata, and spinal cord in MJD is comparable to that commonly seen in terminal SCA2 and SCA7 patients, provide suitable explanations for a variety of less understood clinical MJD symptoms (Riess et al, 2008).

1.2.3. Cell death

- *In MJD patients*

The mechanism of cell death in polyQ diseases remains unclear and might be very complex, as many processes triggered by the presence of expanded polyQ proteins can lead to cell death. This phenomenon can be due such as direct activation of cell death pathways, mitochondrial abnormalities, transcriptional dysregulation, proteasome impairment, defects in axonal transport, or unfolded protein response. Other pathophysiological events such as those associated with excitotoxicity, metabolic stress, or accumulation of free radicals may promote the cell fate toward death by further enhancing the mitochondrial dysfunction (Bauer and Nukina, 2009)

Apoptosis has been proposed as a possible mechanism for neuronal death in neurodegenerative diseases (Ekshyyan and Aw, 2004). However, there is no direct and convincing evidence of apoptosis in brains of patients with these disorders, and the mechanisms of neuronal death in most neurodegenerative diseases remain unknown. The mechanisms of pathogenesis in MJD have not been fully clarified. Several lines of evidence have suggested that the apoptotic machinery can be triggered by the expansion of polyglutamine stretches which MJD mutant protein contains (Ikeda et al,1996). Based on that, Kumada and co-workers examined the occurrence of apoptotic cell death using terminal deoxynucleotidyl-transferase (TdT)-mediated *in situ* nick end labelling (TUNEL) assay in brains obtained at autopsy from MJD patients, and immunohistochemically investigated the *in situ* expression of apoptosis-related proteins. These authors found an augmentation of Bcl-x (Bcl-xS and Bcl-xL) expression, well known apoptosis-related proteins in the Purkinje cells of three cases (Kumada et al, 2000). However they found this result intriguing once Bcl-xS is a proapoptotic protein and Bcl-xL is a well characterized antiapoptotic protein. Nevertheless, more recent studies demonstrated that expression ataxin-3-Q79 in cultured CNS rat neurons causes

an upregulation of Bax mRNA level and downregulation of Bcl-xL mRNA levels (Chou et al, 2006). One case of MJD showed TUNEL-positive granular cells in the cerebellar cortex (Kumada et al, 2000).

The upregulation of inflammatory genes in cell lines expressing expanded *ATXN3* was confirmed by detection of neuroinflammatory markers in the pons of MJD patients, suggesting that glia contribute to MJD pathogenesis (Evert et al, 2001). The precise role of glia in the pathogenic mechanism of MJD is largely unexplored. However, studies in a transgenic mouse model for MJD in 2010, reported that glial cells were not primed for activation before the onset or in early stages of the disease, suggesting that glial activation observed in *post-mortem* tissues could be a consequence rather than a cause of a long neurodegeneration process undergone by human patients (Silva-Fernandes et al, 2010). Systematic temporal and functional analysis of the several types of glial cells in brains from MJD patients and MJD mouse models will help to understand their specific role during the development of this disease.

- *In mouse models of MJD*

Some mouse models of MJD developed so far demonstrated neurodegeneration of specific affected regions overlapping those affected in human MJD patients. Moreover, despite several MJD mouse models having been generated, only some of them demonstrated neurodegeneration in specific regions of the brain (table 5). The first transgenic mouse model of MJD expressing truncated cDNA of the *ATXN3* gene under the control of the L7 promoter of Purkinje cells showed an atrophic cerebellum and massive loss of Purkinje cells, which are not primarily affected in MJD (Ikeda et al, 1996). In 2002, pathological examination of the brains of YAC-transgenic mice carrying the full genomic region of the *ATXN3* gene with expanded (CAG)_n alleles showed degeneration and mild gliosis of the dentate and pontine nerve nuclei. These findings were consistent with the pathological findings reported in MJD patients, where the degeneration of these regions also involves neuronal loss and gliosis. Surprisingly, immunostaining against the astrocytic marker GFAP confirmed the presence of increased numbers of reactive astrocytes also in the cerebellar white matter of symptomatic mice. There was atrophy of the cerebellar Purkinje and molecular cell layers, which was influenced by CAG repeat length and gene dosage (Cemal et al, 2002). In 2004, a transgenic mouse model expressing human mutant (Q71) ataxin-3 under the control of the mouse prion promoter demonstrated a 38% decrease of

dopaminergic neurons (tyrosine hydroxylase [TH]-positive neurons) in the substantia nigra, a region which is also affected in humans. Other brain areas which develop neuronal cell loss in human MJD patients such as the spinal cord, dentate nuclei, pontine nuclei, and to a lesser degree the cerebellar cortex were not altered in this mouse model (Goti et al, 2004). Degenerated Purkinje cells are also observed in human SCA3 patients (Muñoz et al, 2002); in 2010, other mouse model of SCA3 was generated expressing ataxin-3 with 148 CAG repeats under the control of the huntingtin promoter and the authors observed using electron microscopy, darkly stained Purkinje cells, considered as a sign for degeneration in this mouse model at 20 weeks of age (Boy et al, 2010). However, this finding is a little controversial once many neuropathologists consider dark neurons as the most common histologic artefacts (Jortner, 2006). Also in 2010, Silva-Fernandes and co-workers at our lab developed a mouse model of MJD expressing the ataxin with 94 CAG under the control of the CMV promoter and observed neuronal atrophy in the pontine and dentate nuclei and astrogliosis in the vestibular nuclei and substantia nigra. However, and in spite of its neurological phenotype, no cell death (apoptosis or necrosis) and no signals of microglial activation or neuroinflammatory response were observed in the brains of this transgenic mouse (Silva-Fernandes et al, 2010).

Table 5. Neuronal loss observed in MJD mouse models (adapted from Ikeda et al, 1996; Cemal et al, 2002; Goti et al, 2004; Bichelmeier et al, 2007; Silva-Fernandes et al, 2010).

Mouse models	Neurodegeneration	Use of unbiased stereology
Q79-C	Atrophic cerebellum (H&E staining) and massive Purkinje cell loss (IHC anti calbindin)	No
MJD84.2	Decrease in pontine and dentate nuclei neurons (H&E staining) Purkinje cell loss marked by observations of empty baskets (IHC anti-Calbindin) Increased number of glial cells in dentate nucleus and cerebellar white matter (IHC anti-GFAP)	No
Homozygous Q71C	38% fewer (TH)-positive neurons in substantia nigra (IHC anti-TH) No statistically significant differences were found in the total number of neurons in dentate nucleus (Nissl staining)	Yes
70.61	Empty baskets around Purkinje cells indicative of Purkinje cell loss (IHC anti-phosphorylated neurofilament)	No
CMVMJD94	Increased number of glial cells in substantia nigra e vestibular nuclei (IHC anti-GFAP)	Yes

For the mouse models of MJD generated so far, stereological characterization of the brain has not been extensively performed. Goti and co-workers performed unbiased stereology in order to quantify the specific neuronal loss and show that the homozygous Q71C mice showed 38% fewer (TH)-positive neurons in the substantia nigra (Goti et al, 2004). Also in hemizygous-CMVMJD94 mice, unbiased stereology was performed to quantify GFAP-positive cells in the substantia nigra and in the vestibular nuclei, where an increased number of glial cells was found (Silva-Fernandes et al, 2010).

In summary, the mechanisms that cause selective neurodegeneration in MJD are poorly understood and until the moment no model has yet successfully reproduced the specific neuronal loss observed in humans. Indeed, some transgenic mouse models developed motor symptoms in the absence of neuronal cell death (Bichelmeier et al, 2007; Silva-Fernandes et al, 2010). This fact is in agreement with the slow progression of polyQ disorders, in which it is unlikely that neuronal cell death could be the responsible for symptoms early in the course of disease; instead, it could be a final stage after a long period of neuronal dysfunction.

1.2.4. Genetics

In 1993, the MJD locus was mapped in the long arm of chromosome 14 (14q24.3-q32) (Takiyama et al, 1993). One year later, it was found that expansion of CAG repeat motif at the *MJD1* gene, mapped on the long arm of chromosome 14 was present in all affected people of a pathologically confirmed MJD family. In 2001, it was discovered that *MJD1* gene spanned around 48 kb and contained 11 exons, the CAG stretch being located in the exon 10 (Figure 2) (Ichikawa et al, 2001). Nowadays, the official symbol for this gene is *ATXN3*, although *MJD* and *MJD1* are still commonly used (Bettencourt and Lima, 2011).

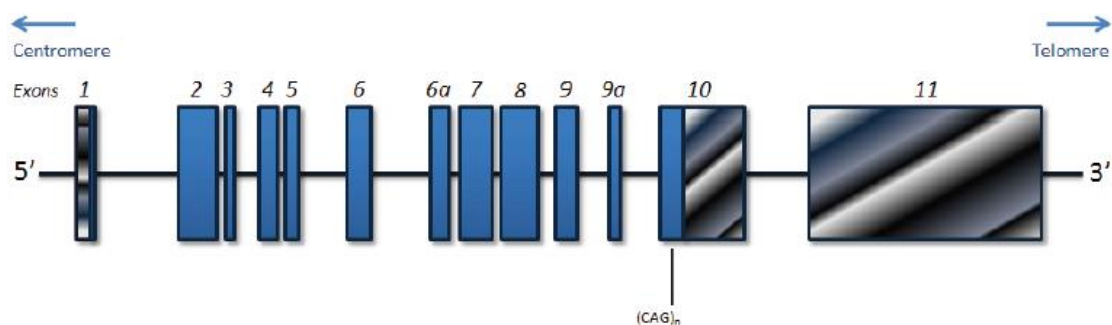


Figure 2. Representation of *ATXN3* gene structure. Exons are numbered from 1 to 11. Blue boxes indicate translated regions; horizontal boxes represent the 5'-untranslated region (UTR) and diagonal boxes correspond to the 3'-UTR. The location of the polymorphic (CAG)_n tract is indicated (Bettencourt and Lima, 2011).

ATXN3 is ubiquitously expressed in the CNS and in the peripheral tissues (Trottier et al, 1998). Low levels of *ATXN3* mRNA are also present in glial cells (Nishiyama et al, 1996). Neurons susceptible to cell death in MJD patients do express *ATXN3*, although not selectively. The cellular *ATXN3* mRNA level does not correlate with clinical severity or pathological involvement. Expression levels of CAG repeats in MJD patients and normal controls do not differ, indicating that the pathogenesis of MJD may involve direct toxicity to vulnerable subsets and/or region-specific co-factors of MJD proteins (Nishiyama et al, 1996).

1.2.5. Ataxin-3

In normal individuals, ataxin-3 has an approximate molecular weight of 42 kDa. However, it is significantly larger in MJD patients, since the elongation of CAG repeat results into an expanded polyQ stretch. This polyQ tract is located in the C-terminus region of the protein, that is variable in length, depending on the isoform (Kawaguchi et al, 1994).

Ataxin-3 is an ubiquitin-binding protein with ubiquitin hydrolase activity *in vitro* (Burnett et al, 2003), proposed to be related with ubiquitin proteasome pathway (UPS) and with transcription regulation. This mutant protein is expressed in neuronal and non-neuronal tissues and when the polyglutamine sequence is expanded it tends to aggregate within cells forming neuronal nuclear inclusion bodies (NNIs). NNIs are frequently observed in brain tissue of MJD patients and are regarded as an important morphological hallmark of the neurodegeneration process in animal models (Paulson et

al, 1997; Seidel et al, 2010). NNIs are ubiquitinated and contain other proteins, namely members of the quality control systems, such as proteosome constituents, ubiquitin and molecular chaperones, as well as transcription factors. The precise role of NNIs on the neurodegeneration that occurs in MJD remains unknown (reviewed in Seidel et al, 2010). This fact restricts our understanding of the mechanisms by which the mutated protein leads to the selective neuronal death profile. However, since NNIs are present in degenerated as well as spared regions of the brain of patients with advanced MJD, NNIs are not thought to be directly pathogenic in affected nerve cells (Arrasate et al, 2004; Rüb et al, 2006).

Recent studies have shown that neuronal demise may be caused by gain of a toxic function of the monomeric mutant ataxin-3, by the partial loss of ataxin-3 function and/or by the toxic effects of soluble amyloid-like oligomers formed by the aggregation of the protein (Matos et al, 2011). However, further knowledge about ataxin-3 biology, the way that it functions, as well about the role it plays in normal cell physiology is much needed.

1.2.6. Mouse models

The identification of the disease causative gene *ATXN3* has made possible the development of animal models for use in studying the mechanisms of pathogenesis of MJD. Mice are the preferred animal model because they are small, short-lived and can be generated in relatively large numbers, kept in a controlled environment, and be used for invasive procedures. Being mammals, they have important genomic, anatomical and physiologic similarities to humans. The problems encountered in the use of patient brain tissue, such as autolysis caused by long post-mortem delays and possible effects of hypoxia or inflammation associated with the immediate causes of death (in MJD, most often respiratory failure due to immobility-associated respiratory tract infections) rather than by the neurological disease process itself can be avoided using mouse models (Colomer, 2005).

Animal models of MJD have been established in order to study the molecular pathway(s) involved in the process of neurodegeneration (table 6) as well as for the assessment of pre-clinical therapeutic trials. The first transgenic mouse model of MJD was generated expressing truncated and full-length cDNA of the *ATXN3* gene under the control of the L7 promoter of Purkinje cells (poorly affected in MJD). No ataxic

phenotype was observed at 23 weeks of age in animals expressing the full-length ataxin-3 with 79Q whereas animals expressing the polyQ fragment displayed an ataxic behaviour at 4 weeks of age and presented an atrophic cerebellum and massive loss of Purkinje cells. This work showed that the expanded polyglutamine tract is *per se* responsible for neuronal loss and degeneration (Ikeda et al, 1996).

In 2002, Cemal and co-workers generated transgenic mouse models using the yeast artificial chromosome (YAC) containing the full-length human *MJD1* gene coding for all alternative spliced isoform of mutant ataxin-3, with 64 to 84 CAG repeats, under the control of the endogenous *MJD1* promoter. These mice with expanded alleles demonstrated a mild and slowly progressive cerebellar deficit, manifesting the symptoms at 4 weeks of age. As the disease progressed, pelvic elevation became markedly flattened, accompanied by hypotonia, and motor and sensory loss. NII formation and cell loss was prominent in the pontine and dentate nuclei, with variable cell loss in other regions of the cerebellum from 4 weeks of age; animals also displayed peripheral nerve demyelination and axonal loss at 26 weeks of age. This mouse was the first model described expressing the full-length *MJD1* gene under the control of its own regulatory elements. However, the phenotype that these mice exhibited was considered too mild for use in therapeutic trials (Cemal et al, 2002).

In 2004, another transgenic mouse model was generated expressing human mutant (Q71) ataxin-3 under the control of the mouse prion promoter. Q71 transgenic mice expressing mutant ataxin-3 above a critical level developed a phenotype including progressive postural instability, gait and limb ataxia, weight loss, premature death, neuronal intranuclear inclusions, and decreased tyrosine hydroxylase-positive neurons in the substantia nigra. Interestingly, a C-terminal cleavage fragment of the transgene product has been revealed in this model, which the researchers also observed in human patients' post-mortem brains (Goti et al, 2004).

Three years later, Bichelmeier and co-worker generated a new transgenic mouse for SCA3 using full-length ataxin-3 cDNA constructs containing 15, 70 and 148 CAG repeats, expressed under the regulation of the mouse prion promoter. Transgenic mice of ataxin-3 with expanded polyglutamine repeats were severely affected by a strong neurological phenotype with tremor and wide-based hindlimbs, as well as markedly reduced motor and exploratory activity, a hunchback, and premature death at 3 to 6 months of age. Q148 mice displayed a more severe neurological phenotype with more inclusions and earlier death when compared with mice expressing mutant ataxin-3 with

70 CAG repeats. The authors proved that the nuclear localization of the mutant protein is crucial for pathogenesis to occur, by the manipulation of the ataxin-3 cellular localization with a NLS (Nuclear Localization Signal) or NES (Nuclear Export Signal) (Bichelmeier et al, 2007).

In 2008, a transgenic mouse model was developed expressing human polyglutamine-expanded ataxin-3-Q79 under the mouse prion promoter. Ataxin-3-Q79 was expressed in cerebellum, pontine nucleus and substantia nigra. Ataxin-3-Q79 transgenic mice displayed motor dysfunction with an onset age of 5-6 months, and neurological symptoms deteriorated in the following months. Prominent neuronal loss was not found in the cerebellum of 10 to 11-month-old ataxin-3-Q79 mice displaying pronounced ataxic symptoms, suggesting that instead of neuronal death, ataxin-3-Q79 caused neuronal dysfunction in the cerebellum and ataxia by disrupting the normal pattern of gene transcription (Chou et al, 2008).

In 2010, Boy and co-workers generated a mouse model of SCA3 expressing ataxin-3 with 148 CAG repeats under the control of the huntingtin promoter, resulting in ubiquitous expression throughout the whole brain. The model showed many features of the disease, including a late onset of symptoms and CAG repeat instability in transmission to offspring. They observed hyperactivity during the first months (not observed in MJD patients) and decline of motor coordination after about 1 year of age. Few and small intranuclear aggregates appeared first at the age of 18 months, further supporting that neuronal dysfunction precedes the formation of intranuclear aggregates (Boy et al, 2010).

In 2010, our group developed a mouse model for MJD expressing the isoform ataxin-3c with 94 CAG under the control of the CMV promoter, resulting in a widespread expression. The model showed reduced balance and coordination, and a very mild locomotor hypoactivity. This mouse model showed intergenerational instability of the CAG repeat and a tissue-specific increase in the somatic mosaicism of the repeat with aging. Histopathological analysis of these MJD mice at early and late stages of the disease revealed neuronal atrophy and astrogliosis in several brain regions (Silva-Fernandes et al, 2010).

Table 6. Brain Pathology of the Mouse Models for MJD (adapted from Colomer, 2012).

Mouse model reference	Severity of behaviour	Intranuclear inclusions in neurons (NI)	Neurodegeneration			Severity of pathology
			Decrease in number of neurons dyed or immuno stained	Increase in number of glial cells immuno stained	Abnormal morphology	
Ikeda et al, 1996	High	ND	ND	ND	Yes*	Intermediate
Cemal et al, 2002	Intermediate	Yes	Yes	Yes	Yes	Intermediate
Goti et al, 2004	High	Yes	Yes	ND	ND	High
Bichelmeier et al, 2007	High	Yes	Yes	NR	Yes	High
Chou et al, 2008	Intermediate	Yes	No	NR	Yes	Intermediate
Boy et al, 2010	Low	Yes	NR	NR	Yes	Low
Silva-Fernandes et al, 2010	Low	No	NR	Yes	Yes	Low
Silva-Fernandes et al, (submitted for publication)	Intermediate	Yes	Yes	ND	Yes	Intermediate

*Neuronal intranuclear inclusions detected in pons, cerebellar nuclei, substantia nigra, and/or Purkinje cells. Evidence of neurodegeneration reported as: a) decrease in number of neurons of pons, dentate nuclei, substantia nigra, and/or Purkinje cells stained with dye or antibody; b) Increase in number of glial cells immunostained in pons, dentate nuclei, substantia nigra, and/or the rest of cerebellum; and c) abnormal morphology of neurons in pons, dentate nuclei, substantia nigra, and/or Purkinje cells. They are included as present (Yes), absent (No), not reported (NR), or not determined (ND). Severity of pathology (last column) is based on whether neuronal intranuclear inclusions (NI) and/or any evidence of neurodegeneration (ND) were detected.

*Only reported in Purkinje cells.

Various mouse models have been generated using methods such as the induction of highly expanded polyglutamine tracts, an increase of transgene copy number, and the use of specific promoters. These mouse models indicate that the CAG repeat length, which is responsible for MJD in humans, is not sufficient for creating the equivalent disease conditions in mice. In order to mimic selective neuronal degeneration of CAG repeat diseases in mice, it may be necessary to express a much higher level of mutant protein with a proper spatio-temporal pattern in the brain. The short lifespan of mice, or possibly high levels of metabolic activity directed against the mutant proteins may partly explain the fact that until now no model fully represents the neuropathologic changes observed in humans (Yamada et al, 2008).

1.2.7. A new mouse model: CMVMJD135

Recently, our group has generated a transgenic mouse model, CMVMJD135, expressing ataxin-3 carrying 135 glutamines under the control of the CMV promoter. With the increase of CAG repeats to 135 in the human ataxin-3 protein (ATXN3) expressed by transgenic animals (CMVMJD135), we have successfully established a mouse model carrying several neurological symptoms of MJD that appear gradually along the disease progression.

CMVMJD135 mice manifest MJD-like motor symptoms beginning at 6 weeks, when they present loss of limb strength, given by a significant decrease in the time in the hanging-wire-grip and in the vertical pole test. At 10 weeks of age, animals developed a balance deficit in the beam test and at 20 weeks of age they displayed motor uncoordination in the rotarod, in addition to tremors and limb claspings at 19 weeks of age. Locomotor and exploratory activity was decreased in transgenic mice at this stage. At 12 weeks of age the gait analysis demonstrated that transgenic animals exhibited foot dragging and at more advanced ages, 16 weeks, swimming uncoordination and a shorted step (figure 3) (Silva-Fernandes et al, submitted for publication).

Histopathological observation of brain sections of transgenic CMVMJD135 mice sacrificed at the age of 24 weeks revealed the presence of shrunken cells (violet cresyl staining) in several regions, such as the pontine nuclei, vestibular nuclei and substantia nigra in comparison with normal cells observed in wild-type animals. No

apoptotic cells were found in the affected brain areas of CMVMJD135 mice at this age by TUNEL assay. Autophagy, also an important process for degradation of protein aggregates was evaluated in the brainstem of CMVMJD135 and no alterations in the autophagy activation were found (Silva-Fernandes et al, submitted for publication).

Immunohistochemistry (IHC) with anti-ataxin-3 and ubiquitin antibodies showed the presence of inclusions in the nucleus of neurons in CMVMJD135 mice brains. Inclusions were observed in different regions of the CNS including the pontine nuclei, lateral reticular nucleus, deep cerebellar nuclei, as well as in non-affected regions such as ventral tenia tecta and olfactory anterior nuclei (Silva-Fernandes et al, submitted for publication). This is concordant with what is been seen in human MJD patients where neurodegeneration is not clearly correlated with the occurrence of ataxin-3 immunopositive inclusions (Rüb et al, 2006).

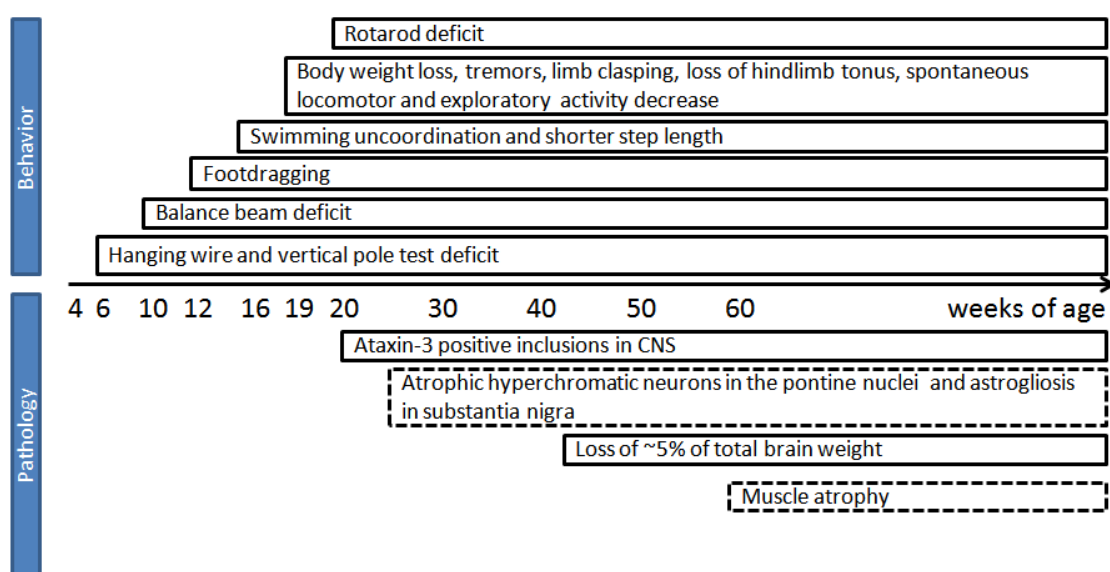


Figure 3. Summary of behaviour and pathology findings in CMVMJD135. The dotted lines indicate unknown age of initiation of atrophic hyperchromatic neurons in pontine and astrogliosis in substantia nigra as well muscle atrophy.

2. OBJECTIVES

2. OBJECTIVES

Taking into account the results observed in animals models for MJD it seems that neuronal cell death could be a final stage after a long period of neuronal dysfunction. In this manner, neuronal cell death observed in post-mortem brain patients - whether apoptotic or nonapoptotic - probably occurs when neurons can no longer tolerate irreversible and widespread dysfunction of multiple cellular pathways. There is a need for the definition of early and late neuropathologic changes in MJD as hallmarks that we can use to assess the efficacy of therapeutic compounds, in addition to the behavioural endpoints (neurological function tests) in animal models of neurodegenerative disease.

Thus, the objectives of this work were:

- i) To determine the volumes of brain regions affected in MJD in the CMVMJD135 mouse model: pontine nuclei, substantia nigra, locus coeruleus and dentate nuclei, and to assess the cerebellar cortex (molecular and granular) layer thickness rather than volume.
- ii) To quantify the number of cells in the brain regions with volume alteration in the previous task.
- iii) To evaluate the type of cells which are quantitatively altered (astrocytes or neurons) when the total cell number was altered.

3. MATERIAL AND METHODS

3.1. Animals

All animals were maintained under standard laboratory conditions: an artificial 12 h light/dark cycle (lights on from 8:00 to 20:00 h), with an ambient temperature of 21 ± 1 °C and a relative humidity of 50–60%; the mice were given a standard diet (4RF25 during the gestation and postnatal periods, and 4RF21 after weaning, Mucedola SRL, Settimo Milanese, Italy) and water *ad libitum*. Health monitoring was performed according to FELASA (Federation for laboratory animal science associations) guidelines (Nicklas et al, 2002), confirming the Specified Pathogen Free health status of sentinel animals maintained in the same animal room. All procedures were conducted in accordance with European regulations (European Union Directive 86/609/EEC). Animal facilities and the people directly involved in animal experiments were certified by the Portuguese regulatory entity — Direcção Geral de Veterinária. All of the protocols performed were approved by the joint Animal Ethics Committee of the Life and Health Sciences Research Institute, University of Minho, and the Institute for Molecular and Cell Biology, University of Porto.

3.2. DNA extraction and mouse genotyping

DNA from mouse tail biopsy (~5 mm) was isolated using a Citogene Kit (Citomed). Tails were digested overnight with 300µL of Cell Lysis buffer (Citogene Kit, Citomed) and 2µL of Proteinase K (Citogene). Then we added 100 µL of protein precipitation solution (Citogen Kit, Citomed), vortexed for 20 seconds followed by a centrifugation at 13000 rpm during 8 minutes. The supernatant was suspended in 300 µL of isopropanol and then centrifuged again at 13000 rpm during 8 minutes. The pellets were washed in 70% ethanol and centrifuged at 13000 rpm for 2 minutes. The pellets were eluted in 30 µL DNA Hydration solution (Citogene Kit, Citomed).

In a single PCR genotyping tube we used 6,25 µL of Supreme Master Mix 2x Green (NZYtaq, NZYTech), 1µL of the primers TR6 (5'-TACATCAATGGGCGT GGAT-3') and TR7 (5'-GAGGTCAAACAGCGTGGA-3') at the concentration of 10 µM to amplify the transgene (454 bp), and 0,5 µL of the primer mmMJD89 (5'-GCTAGCTAGAGCTACTTATTG-3') and mmMJD54 (5'-GACTCCAGAGAGCAC CTG-3') at the concentration of 10 µM to amplify the mouse homologous *ATXN3* gene

(800 bp) as an internal control of the PCR. The DNA was added at a concentration of 100ng/μL. The PCR conditions were as follows: 95°C, for 10 minutes, 35 cycles: 1 minute of denaturation step at 95°C, annealing at 60°C and elongation at 72°C. The final elongation was at 72°C for 5 minutes. The PCR product was hold at 4°C.

Amplification products were visualized in 1,5% (W/V) agarose gel and electrophoresed at 120 Volts for 20 minutes. Gels were analysed in Gel Doc™ EZ Imager (BIO RAD) by the Image Lab™ Software version 4.1.

3.3. Molecular analysis of the (CAG)_n repeat

In a single tube, 2,5 μL of 10x High Fidelity PCR Buffer + MgCl₂ (Fermentas), 0,4μL of 10mM dNTP's (NZYTech), 0,5 μL of the primer MJD25a at the concentration of 6,6 ng/μL (5'-GGCTGGCCTTTCACATGGAT-3'), 0,5 μL 6-FAM fluorescently-labeled MJDcDNA primer at 6,6ng/μL (5'-CGGAAGAGACGAGAAGCCTAC-3'), 1,25 μL of DMSO 100% and 0,2 μL of Taq High Fidelity enzyme (Fermentas). The genomic DNA was used at a concentration of 25ng/μL. The PCR parameters were as follow: 95°C, for 10 minutes, 35 cycles: 1 minute of denaturation step at 95°C, annealing at 60°C and elongation at 72°C. The final elongation was at 72°C for 5 minutes. The PCR product was hold at 4°C. Amplification products were visualized in 1,5% (W/V) agarose gel electrophoresis and gels were analysed in Gel Doc™ EZ Imager (BIO RAD) by the Image Lab™ Software version 4.1.

Products were displayed in an ABI 310 automated DNA sequencer (Applied Biosystems, Foster City, CA). The major allele size was determined by densitometry using AlphaEase software to detect the peak with the highest height in the AlphaImager 2200 (AlphaInnotech). The CAG tract length of the major size band was determined using an equation from the calibration curve obtained with cloned alleles containing known numbers of CAG repeats (Williams et al, 1999).

3.4. Stereology

3.4.1. Tissue preparation and staining

At 60 weeks of age, CMVMJD135 (n=9) and wild-type (n=6) mice were deeply anaesthetized: ketamine hydrochloride (150 mg/kg) plus medetomidine (0,3 mg/kg);

and transcardially perfused with 4% paraformaldehyde (PFA) in phosphate buffered saline (PBS). The brains were removed, blocked in the coronal plane and processed in glycomethacrylate (Tecnovit 7100). Approximately 4 weeks post-processing, brains were sectioned at 30 μm in the coronal plane with a rotating microtome and wet mounted on gelatinized slides. The sections were stained with 10% Giemsa stain, mounted with Entellan-New (Merck) and coverslipped.

3.4.2. Design-based stereology

Design-based stereological estimates of neuronal number and regional volume were obtained by systematic random sampling in pontine nuclei (Bregma level - 3.80 mm through - 4.60 mm), substantia nigra (Bregma level - 2.46 mm through - 4.04 mm), dentate nuclei (Bregma level - 5.68 mm through - 6.36 mm) and locus coeruleus (Bregma level - 5.34 mm through - 5.80 mm) according to the Paxinos and Franklin mouse brain atlas of 2001. The above-mentioned regions were outlined based on noticeable citoarchitectural differences, namely density of cells. Stereological procedures were performed blind to the observer.

3.4.3. Cavalieri's principle: Volume estimation

The Cavalieri's method was used to assess the volume of regions of interest. The Cavalieri's principle permits an unbiased and accurate volume evaluation of an arbitrary shape and size three-dimensional structure using two-dimensional serial-sections. Estimates of regional volume were obtained based on systematic random point counting (Gundersen and Jensen, 1987). Briefly, every 2 sections were used and the cross-sectional area was estimated by point counting (final magnification 40x). The volume of regions of interest was estimated by counting the number of unique points along a systematic random grid, across the outlined region that fell within the region of interest. Each included point represents a known area, such that the sum of the number of points lying within the boundaries of the region multiplied by the corresponding area and also multiplied by the represented thickness yields an estimate of the volume for each animal in cubic microns. Thus, multiplying the distance between sections by their total cross-sectional area give us a volume that leads to precise MRI-like results.

Measurements were performed using the Visiopharm Integrator System, version 2.12.3.0 and a camera (Pixelink PL – A622) attached to a motorized microscope (Olympus BX51) using a 40X, 0.16 numerical aperture oil immersion objective.

3.4.4. Fractionator: neuronal number estimation

Average cell number was estimated using the optical fractionator method. The optical fractionator is a combination of the optical dissector, a three-dimensional probe used for counting, and fractionator sampling a scheme involving the probing of a known fraction of tissue (West et al, 1991). Three sampling fractions are used with the optical fractionator method. First, the section sampling fraction (ssf) represents the proportion of microscopical sections of the entire, serially sectioned brain structure that is sampled for evaluation. The area sampling fraction (asf) corresponds to the proportion of the sectional area that is investigated within the sampled sections. And, finally, the height (h) of the dissector is known relative to the thickness of the sections (t) and captures the part of the investigated cross-sectional area of the sampled sections. The estimated total number of particles (N) is obtained by multiplying the total number of cells actually counted in the dissectors ($\sum Q^-$) that fell within the sectional profiles of the subdivision seen in the sampled sections per brain structure (figure 4) (West et al, 1991).

$$N = \sum Q^- \cdot \frac{1}{ssf} \cdot \frac{1}{asf} \cdot \frac{t}{h}$$

Figure 4. Formula of estimation of the total number of cells (West et al, 1991).

The size of the region of interest is implicitly determined from the combination of these fractions. This means that, with the optical fractionator technique, no information on the size of the region of interest or magnification of the microscope is needed. This also implies that this counting technique is independent of e.g. swelling and/or shrinkage of the tissue during processing (West, 1993).

In summary, a grid of virtual 3D-boxes equally spaced was superimposed on every 2th section of interest and we counted the number of cells falling inside it (figure 5).

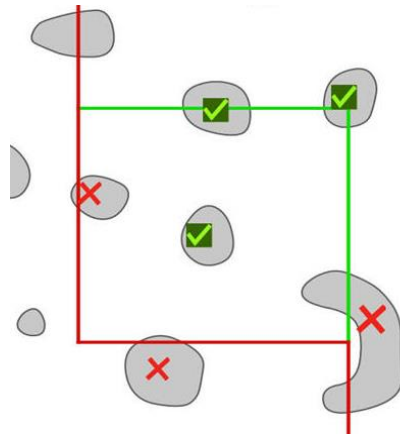


Figure 5. Counting frame of the optical dissector. An object is counted if it lies completely inside the counting frame or if it crosses a green (inclusion) line but not a red (exclusion) line. (adapted from: <http://www.stereology.info/criteria-for-counting-cells/>)

Inclusion and exclusion counting criteria were followed by a blinded observer who recorded counts only when a single cell nucleolus was brought into focus within the dissector frame (Sterio, 1984).

In this study, every second section containing the pontine nuclei, substantia nigra, locus coeruleus and dentate nuclei was selected to obtain a sample in a systematic uniform random manner (section sampling fraction; $ssf=0.5$).

- For **pontine nuclei** and **substantia nigra**: The area (a) of the counting frame was $400 \mu\text{m}^2$ ($20 \mu\text{m} \times 20 \mu\text{m}$), the area sampling fraction (asf) = a (frame) / a (step length) was 0,004. The height (h) of the optical dissector was $15\mu\text{m}$. The yielding for pontine nuclei was 10-13 sections per brain and for substantia nigra was 18-22 sections per brain.
- For **locus coeruleus**: The area (a) of the counting frame was $400 \mu\text{m}^2$ ($20 \mu\text{m} \times 20 \mu\text{m}$), the area sampling fraction (asf) = a (frame) / a (step length) was 0,04. The height (h) of the optical dissector was $15\mu\text{m}$. The yielding was 5-7 sections per brain.

- For **dentate nuclei**: The area (a) of the counting frame was 400 μm^2 (20 $\mu\text{m} \times 20 \mu\text{m}$), the area sampling fraction (asf) = a (frame) / a (step length) was 0,018. The height (h) of the optical dissector was 15 μm . The yielding was 9-11 sections per brain.

The quantification of the total cell number was performed using The Visiopharm Integrator System, version 2.12.3.0 and a camera (Pixelink PL- A622) attached to a motorized microscope (Olympus BX51) using a 400X, 1.0 numerical aperture oil immersion objective.

3.5. Immunohistochemistry

CMVMJD135 transgenic (n=9) and wild-type mice (n=6) with 93 weeks of age were deeply anaesthetized (3mL Imalgène, 600 μL Dorvet and 19,5 mL saline) and transcardially perfused with 4% PFA in PBS. Brains were post-fixed overnight in fixative solution and embedded in paraffin. Representative sections of mice brains were stained with hematoxylin-eosin (H&E) for histological examination. For IHC, slides with 4- μm -thick sections were placed in the incubator at 72°C for 10 minutes to allow the paraffin to melt and then we proceed with the deparaffinization/ hydration protocol. 10mM citrate buffer, pH=6.0 was pre-heated and slides were incubated in the buffer during 20 minutes in the microwaves, at low temperature, in order to allow the antigen retrieval. After that, slides were transferred to dH₂O for 15 minutes and endogenous peroxidase was inactivated by immersing the tissue sections in 3% H₂O₂ in PBS solution for 30 min. Slides were then washed in PBS and PBS-Triton 0,3% and the blocking was performed using V Block solution (Ultravision Plus large volume detection system Anti-polivalent, HRP-Thermo scientific), during 8 minutes.

- For NeuN (Neuronal Nuclei) staining in pontine nuclei, slides were incubated with mouse monoclonal antibodies against neuronal nuclei, NeuN (Chemicon, Millipore) (1:100).

- For GFAP (Glial Fibrillary Acidic Protein) staining in pontine nuclei, slides were incubated with polyclonal rabbit GFAP antibody (DAKO Corporation, Carpinteria, CA) (1:500).
- For TH (Tyrosine-Hydroxylase) staining in substantia nigra, slides were incubated with polyclonal rabbit TH antibody (Chemicon, Milipore) (1:300).

A biotinylated secondary antibody was applied, followed by the streptavidin-biotin peroxidase complex system (Ultra Vision Large Volume Detection System Anti-Polyvalent, HRP; Lab Vision Corporation, Fremont, CA, USA) according to the manufacturer's instructions and with peroxidase-diaminobenzadine to visualize and develop the antigen-antibody reaction and DAB (3,3-diaminobenzidine) substrate (Vector Laboratories Inc., Burlingame, CA, USA). The slides were counterstained with hematoxylin 25% according to standard procedures and analysed with an optical microscope (Olympus, Hamburg, Germany). Finally, they were mounted with Entellan-New (Merck) and coverslipped.

The stereological analysis of GFAP and NeuN positive cells in pontine nuclei and the estimate of TH-positive neurons in substantia nigra (total 3 sections per brain) was performed in sagittal sections using The Visiopharm Integrator System, version 2.12.3.0 and a camera (Pixelink PL- A622) attached to a motorized microscope (Olympus BX51) using a 400X, 1.0 numerical aperture oil immersion objective.

3.6. Estimation of cerebellar layer thickness

Paraffin-embedded sagittal sections were stained with hematoxylin and eosin (H&E) and the thickness of molecular and granular layers of the cerebellum were measured at preculminate fissure (PCFUF) and secondary fissure (SF) in 6 animals (n=3 CMVMJD135 and n=3 wild-type) at 93 weeks of age. One rectangular line was drawn across PCFUF and SF, and 3 perpendicular lines (distant from each other 200 μ m) were drawn in order to measure the thickness of the layers. The measurements of each layer for each animal were averaged. Two sections were measured per animal (figure 6).

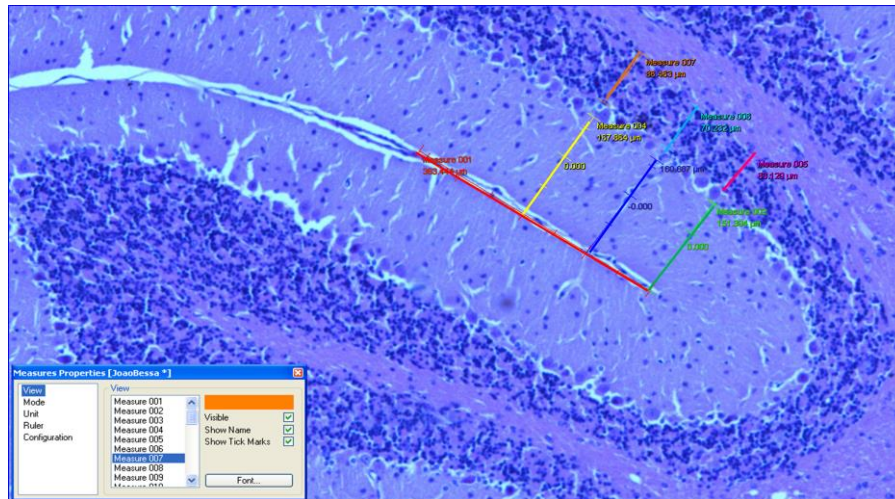


Figure 6. Measurements of molecular and granular layers of cerebellum in secondary fissure.

3.7. Statistical analysis

Continuous variables with normal distribution (K-S test $p > 0.05$) were analysed with the Student t-test. All statistical analyses were performed using SPSS 20.0 and a critical value for significance of $p < 0.05$ was used throughout the study.

4. RESULTS

4.1. Quantification of volume and total number of cells in brain regions known to be affected in MJD.

In this chapter we quantified the total number of cells and determined the volume in the pontine nuclei, locus coeruleus, substantia nigra and dentate nuclei in CMVMJD135 transgenic animals at 60 weeks of age and their wild-type littermates. At this age, CMVMJD135 mice exhibit a well established phenotype characterized by severe motor deficits such as balance deficit, gait ataxia and motor uncoordination. They also present brain pathology characterized by the presence of ataxin-3-positive intranuclear inclusions in several brain regions, namely in the pontine and dentate nuclei (Silva-Fernandes et al, submitted for publication).

Moreover, the analysis of the CAG repeat length of CMVMJD135 mice revealed no variations among animals (average of CAG repeat: 133 ± 1.86).

4.1.1. Pontine nuclei

The pontine nuclei (PN) are a part of the pons involved in motor activity. They allow modification of actions in the light of their outcome, or error correction, and are hence important in learning motor skills. Afferent fibers entering the cerebellum via the middle cerebellar peduncle contain afferents from the cerebral cortex that synapse in the pons. In pons, pontine nuclei project to the opposite side of the cerebellum via the crossed fibers of the middle cerebral peduncle. Forming the largest of the afferent fibers to the cerebellum, the middle cerebellar fibers enter the cerebellum where each axon branches to innervate granule cells. This connection forms the main pathway linking the cerebral cortex to the cerebellum (figure 7) (Bhatnagar, 2002).

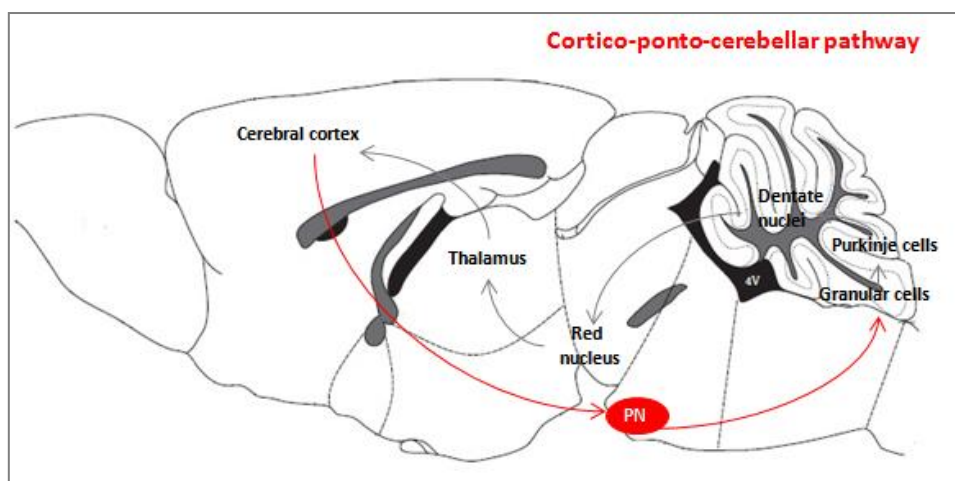


Figure 7. Illustration of cortico-pontine (PN)-cerebellar pathway. The red arrows correspond to cerebellar afferent system (corticopontine and pontocerebellar tracts). The grey arrows correspond to efferent cerebellar projections.

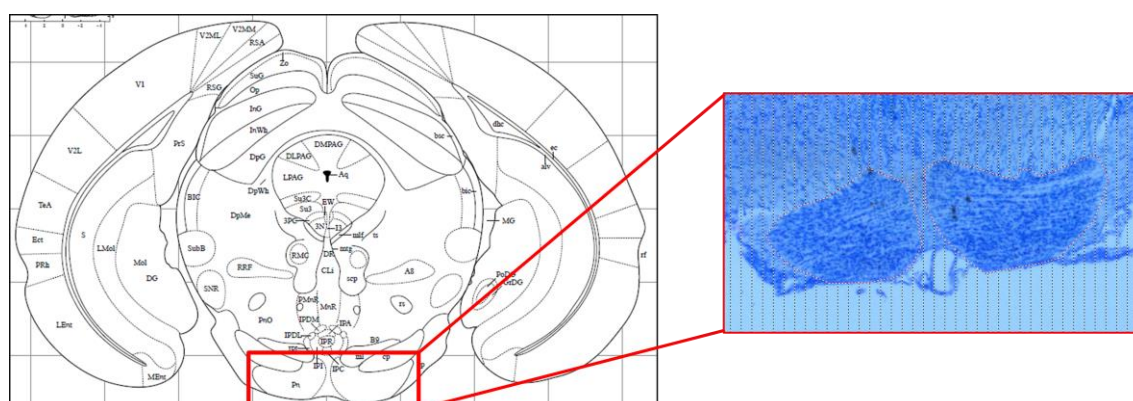


Figure 8. Low magnification micrograph of glycolmethacrylate-embedded coronal section of pontine nuclei of the mouse stained with Giemsa and the corresponding atlas scheme used for delineation of the region.

In order to assess the volume and total number of cells in pontine nuclei, we performed stereological analysis in 5 wild-type animals and 9 CMVMJD135 transgenic animals. Our results revealed a 13% decrease in volume ($p=0.018$) and 12% decrease in total number of cells ($p=0.032$) in pontine nuclei of CMVMJD135 mice when compared to wild-type animals.

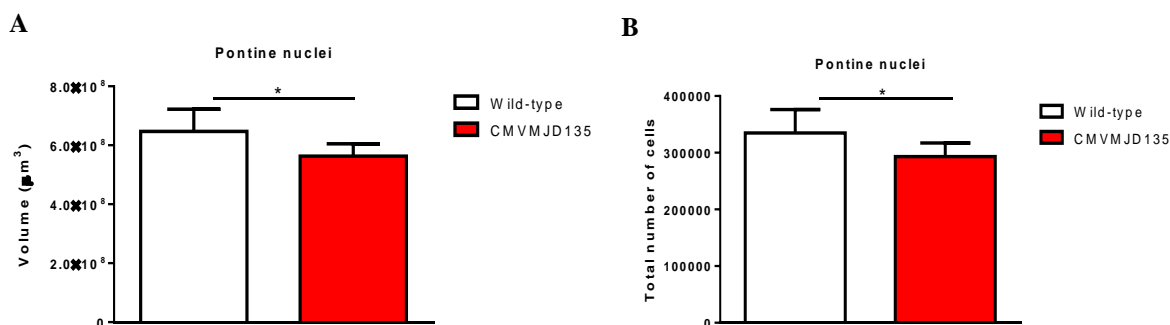


Figure 9. Total volume (A) and total number of cells (B) of pontine nuclei calculated for wild-type (σ n=5) and CMVMJD135 mice (σ n=9). Asterisks indicate significant differences between wild-type and CMVMJD135 mice (* p <0.05). CMVMJD135 showed a loss of volume (13%) and decrease in the number of cells (12%) in pontine nuclei.

4.1.2. Locus coeruleus

The locus coeruleus is located in the posterior area of the rostral pons in the lateral floor of the fourth ventricle. It is composed of mostly medium-size neurons (Berridge and Waterhouse, 2003). Melanin granules inside the neurons of locus coeruleus contribute to its blue color. Locus coeruleus is the principal site for brain synthesis of norapinephrine (noradrenaline). The locus coeruleus and the areas of the body affected by the norepinephrine that it produces are described collectively as the locus coeruleus-noradrenergic system (LC-NA system) (Mehler and Purpura, 2009). The projections of this nucleus reach far and wide. They innervate the spinal cord, the brainstem, cerebellum, hypothalamus, thalamus, the basal telencephalon and the cerebral cortex (figure 10) (Bhatnagar, 2002).

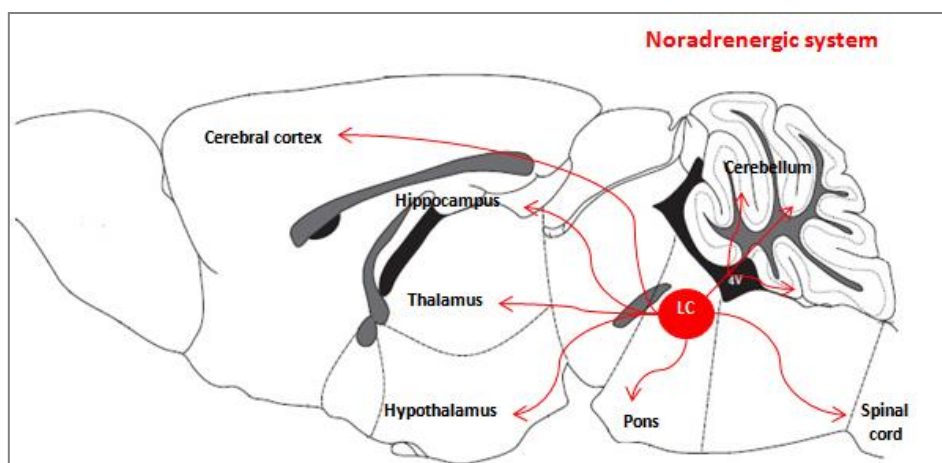


Figure 10. Illustration of the locus coeruleus (LC) – noradrenergic system. The red arrows correspond to the main brain regions involved in the noradrenergic system.

Some of the most important functions influenced by locus coeruleus are neuroplasticity, arousal and sleep-wake cycle, attention and memory, emotions, behavioural flexibility, behaviour inhibition and stress, posture and balance (Benarroch, 2009).

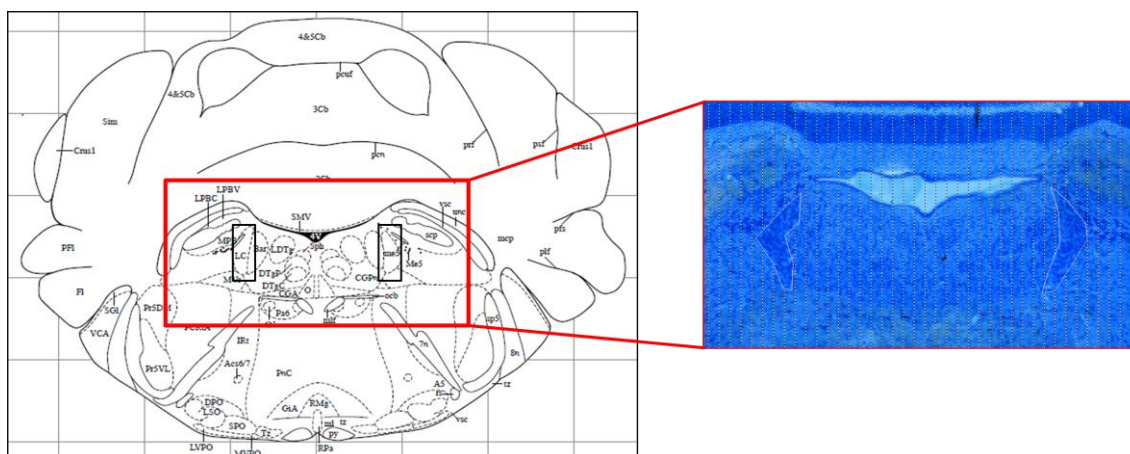


Figure 11. Low magnification micrograph of glycolmethacrylate-embedded coronal section of locus coeruleus of mouse stained with Giemsa and the corresponding atlas scheme used for delineation of the region.

In order to assess the volume and total number of cells in the locus coeruleus, we performed stereological analysis in 5 wild-type mice and 5 CMVMJD135 animals. Our

results revealed a non-significant trend towards a reduction of the volume and total number of cells in CMVMJD135 mice when compared to wild-type animals.

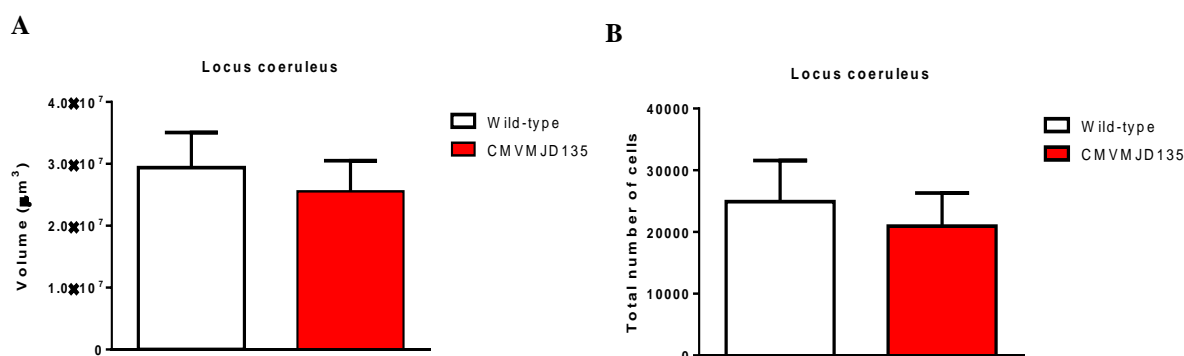


Figure 12. Total volume (A) and total number of cells (B) of locus coeruleus calculated for wild-type (♂ n=5) and CMVMJD135 mice (♂ n=5). CMVMJD135 showed a trend towards a decrease, although not statistically significant, in volume and in the total number of cells in locus coeruleus.

4.1.3. Substantia nigra

The substantia nigra is a brain structure located in the mesencephalon (midbrain) that plays an important role in reward, addiction and movement. The substantia nigra is a large motor nucleus located between the tegmentum and the crus cerebri, and is found throughout the midbrain. The nucleus is composed of medium-size multipolar neurons that possess inclusion granules of melanin pigment within their cytoplasm. The neurons of the substantia nigra are dopaminergic and inhibitory and have many connections to the striatum. It projects axons to the caudate nucleus and the putamen and release dopamine at their terminals as the neurotransmitter (Snell, 2010). Substantia nigra makes part of the main basal ganglia loop which includes other brain areas such as the striatum (caudate nucleus and putamen), globus pallidus and the subthalamic nucleus (figure 13) (Bhatnagar, 2002).

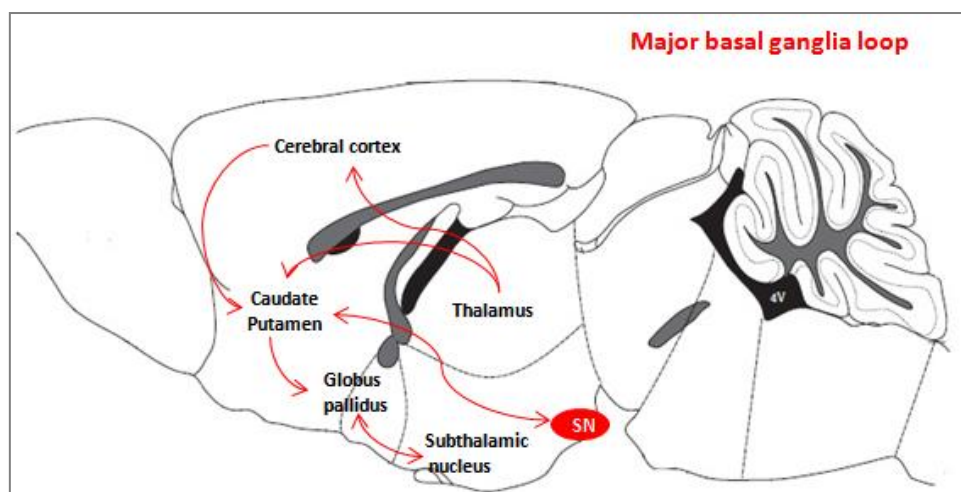


Figure 13. Illustration of the major basal ganglia loop. The red arrows correspond to the principal afferent and efferent fibers forming basal ganglia loops; it includes the dopaminergic projections from substantia nigra (SN) to caudate/putamen.

Although the substantia nigra appears as a continuous band in brain sections, it actually consists of two parts with very different connections and functions: the *pars compacta* and *pars reticulata*. The *pars compacta* serves mainly as an input to the basal ganglia circuit, supplying the striatum with dopamine. The *pars reticulata*, on the other hand, serves mainly as an output, conveying signals to the thalamus and superior colliculus (Deniau et al, 1978).

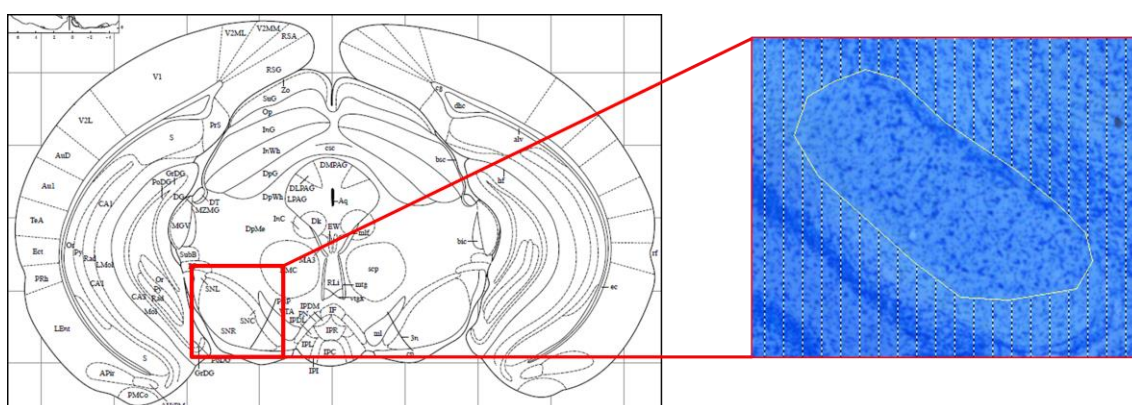


Figure 14. Low magnification micrographs of glycolmethacrylate-embedded coronal section of substantia nigra of the mouse stained with Giemsa and the corresponding atlas scheme used for delineation of the region.

In order to assess the volume and total number of cells in substantia nigra, we performed stereological analysis in 5 wild-type animals and 5 CMVMJD135 mice. Our results revealed no differences in terms of volume and total number of cells in substantia nigra of CMVMJD135 mice when compared to the wild-type control animals.

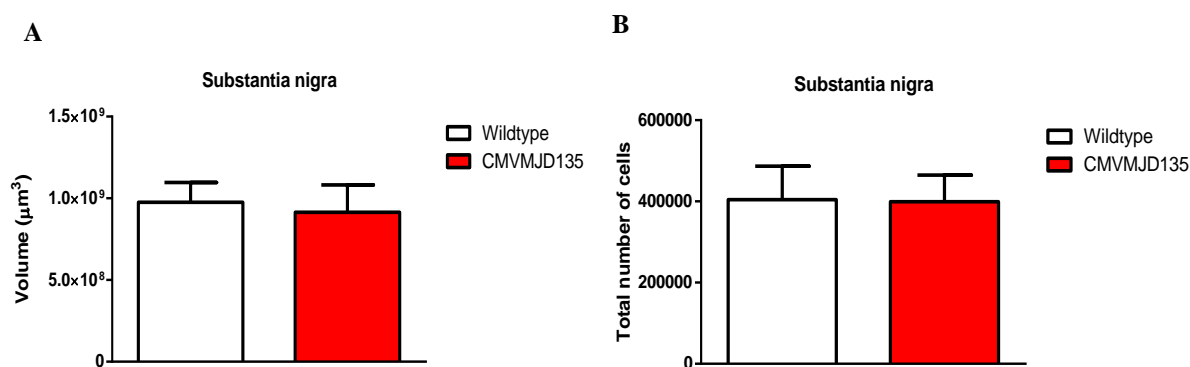


Figure 15. Total volume (A) and total number of cells (B) of substantia nigra calculated for wild-type (σ n=5) and CMVMJD135 mice (σ n=5). CMVMJD135 didn't show differences in terms of volume and total number of cells in substantia nigra.

4.1.4. Dentate nuclei

The dentate nuclei are located within the deep white matter of each cerebellar hemisphere, and are the largest structures linking the cerebellum to the rest of the brain (Snell, 2010). The dentate nuclei are responsible for the planning, initiation and control of voluntary movements. Dentate nuclei receive afferent signals from the motor cortex via the pontocerebellar system and efferent signals via the superior cerebellar peduncle through the red nucleus to the contralateral and ventrolateral thalamus (figure 16) (Bhatnagar, 2002). The dorsal region of the dentate nuclei contains output channels involved in motor function, more specifically the movement of skeletal muscle, while the ventral region contains output channels involved in non motor functions, such as conscious thought and visuospatial function (Sultan, 2010).

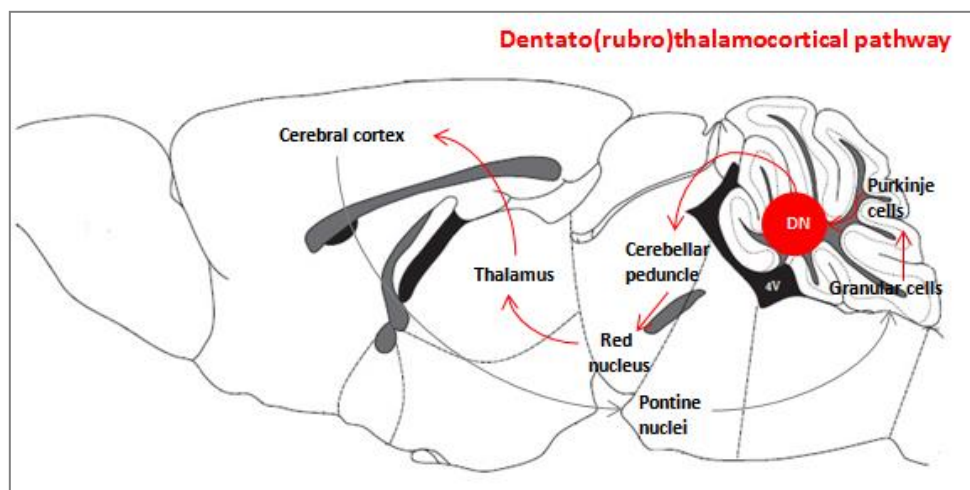


Figure 16. Illustration of the dentato(rubro)thalamocortical pathway. The red arrows represent efferent projections of cerebellum that arise from dentate nuclei (DN) and continue their way to the motor cortex. Grey arrows correspond to the major afferent pathway of cerebellum.

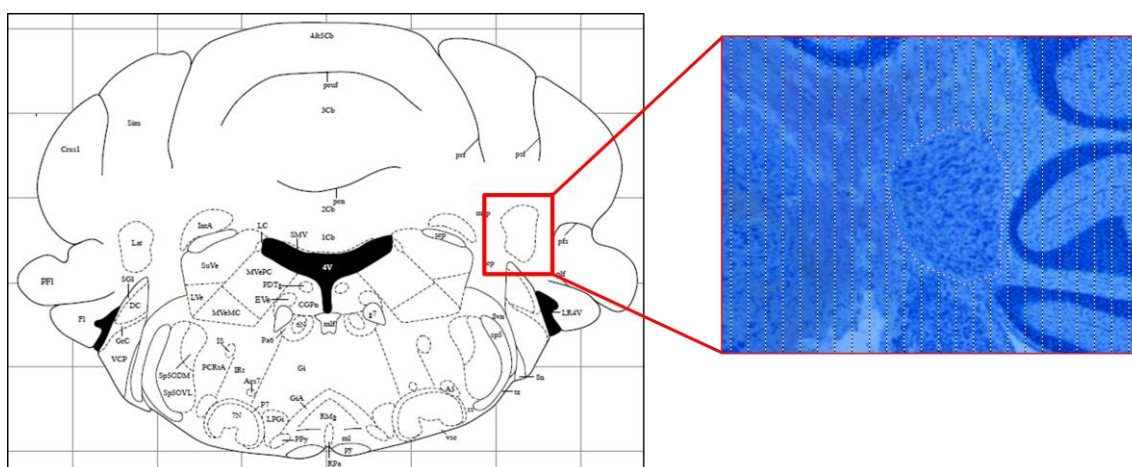


Figure 17. Low magnification micrographs of glycolmethacrylate-embedded coronal section of dentate nuclei of the mouse stained with Giemsa and the corresponding atlas scheme used for delineation of the region.

In order to assess the volume and total number of cells in dentate nuclei, we performed stereological analysis in 4 wild-type mice and 4 CMVMJD135 transgenic mice. No statistically significant differences were observed in terms of total number of cells in this region. However, our results revealed a decrease of 37% in volume of

dentate nuclei ($p=0,0062$) of CMVMJD135 mice when compared to the wild-type animals.

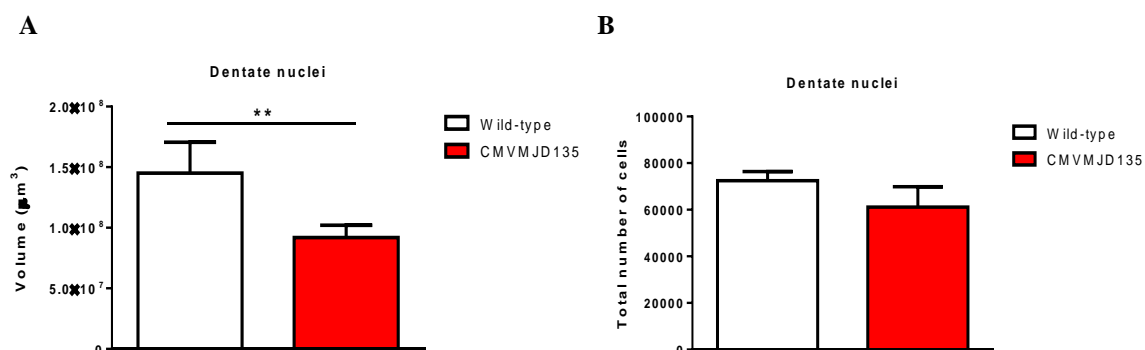


Figure 18. Total volume (A) and total number of cells (B) of dentate nuclei calculated for wild-type (σ n=4) and CMVMJD135 mice (σ n=4). Asterisks indicate significant differences between wild-type control and CMVMJD135 transgenic mice (** $p<0.01$). CMVMJD135 showed a loss of volume (37%) in dentate nuclei and a non-significant decrease in the total number of cells.

4.2. Quantification of specific cell types – neurons and astrocytes – in CMVJD135 mouse brains.

Although extremely complex, the brain is largely constituted of only two main cell types: neurons and glial cells.

Neurons are involved in information transmission – receiving, processing and transmitting information through their highly specialised structure. The majority of neurons are unable to undergo cell division or repair (Snell, 2010). NeuN is a neuronal nuclear antigen that is commonly used as a biomarker for neurons. NeuN immunoreactivity has been widely used to identify neurons in tissue culture and in sections and to measure the neuron/glia ratio in brain regions (Herculano-Houzel and Lent, 2005).

Glial cells are major constituents of the CNS, and while they do not have a direct role in neurotransmission, they play a supporting role that helps define synaptic contacts and maintain the signalling abilities of neurons. Various types of glial cells can be found in the brain; including astrocytes, oligodendroglia and microglia. Glial cells are smaller than neurons and they have well-defined roles such as modulating the rate of nerve impulse propagation; controlling the uptake of neurotransmitters; and playing a pivotal role during development and adulthood (Snell, 2000). Glial fibrillary acidic protein (GFAP) is an intermediate filament (IF) protein that is expressed by numerous cell types of CNS, including astrocytes, astrogliosis being characterized by a rapid increase in the synthesis of GFAP intermediate filaments (Eng et al, 2000).

In this chapter we aimed to determine which type of cells are quantitatively altered in regions that presented altered number of cells (previous results). Thus, we performed IHC in order to stain for neurons (IHC anti-NeuN) and astrocytes (IHC anti-GFAP) in the pontine nuclei of CMVMJD135 transgenic animals at 93 weeks of age and compared with wild-type animals.

Our results revealed no differences in the number of GFAP-positive cells in pontine nucleus of CMVMJD135 mice when compared to wild-type animals (Figure 19). Interestingly, CMVMJD135 mice showed a reduced number, albeit not statistically significant, of NeuN-positive cells in the pontine nuclei (Figure 20).

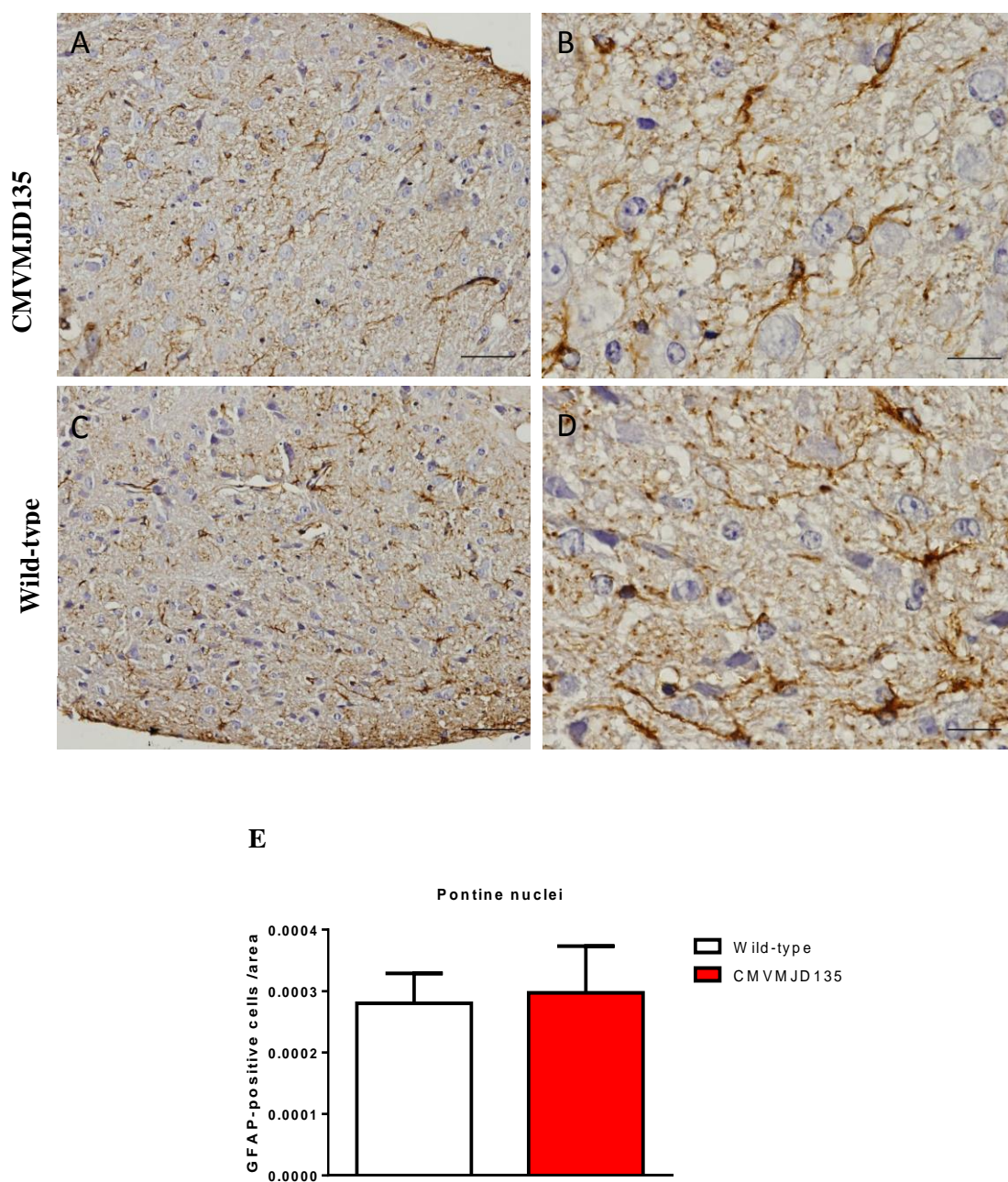


Figure 19. GFAP immunostaining of the pontine nuclei in CMVMJD135 (δ n=5) (A-B) and wild-type (δ n=3) animals (C-D) at late stage of the disease (93 weeks of age); Scale bar: 50 μ m (A and C) and 20 μ m (B and D) and the quantification of the number of GFAP-positive cells calculated for wild-type and CMVMJD135 mice in pontine nuclei (E). CMVMJD135 showed no significant differences in the number of astrocytes.

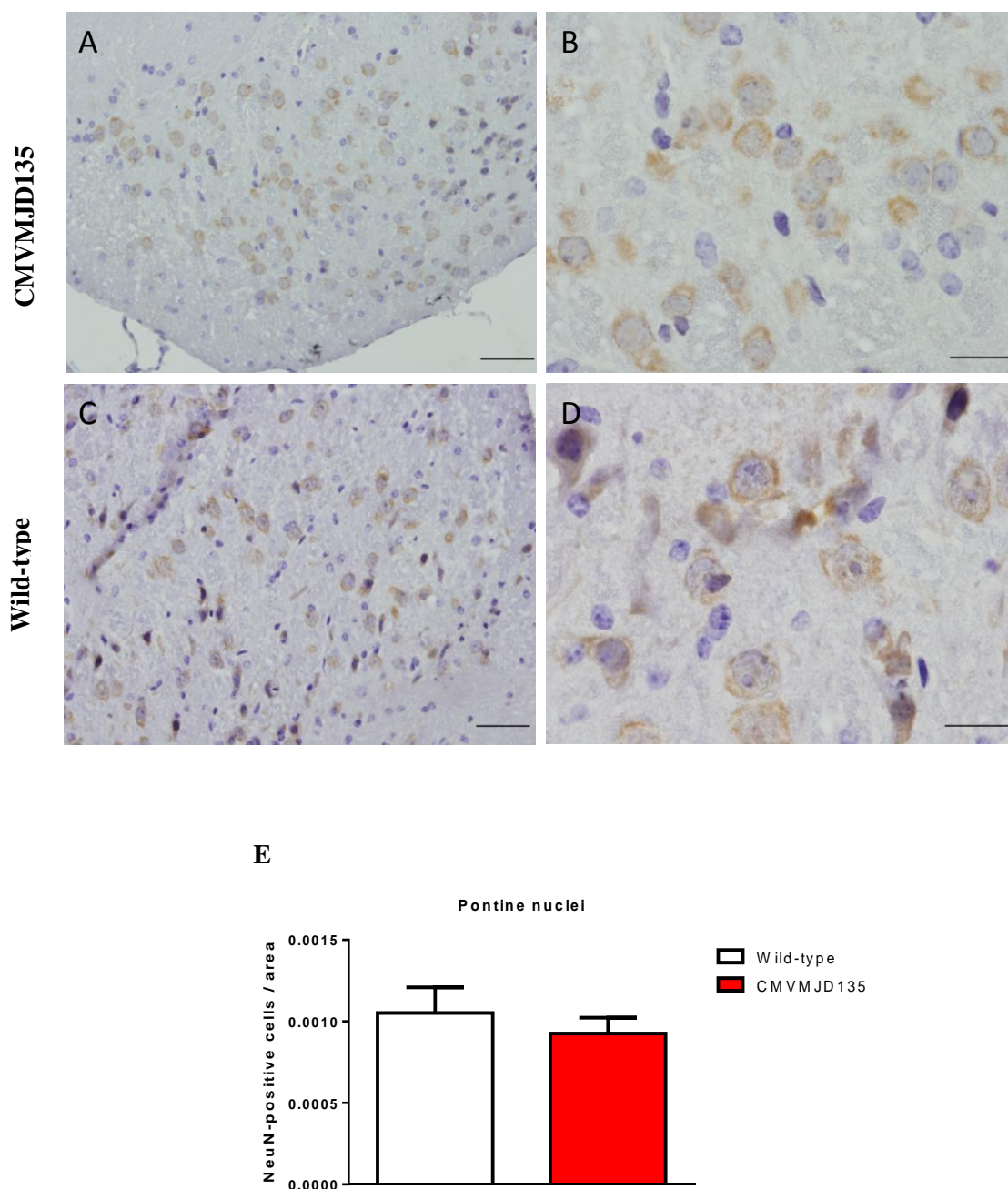


Figure 20. NeuN immunostaining of the pontine nuclei in CMVMJD135 (♂ n=4) (A-B) and wild-type (♂ n=3) animals (C-D) at late stage of the disease (93 weeks of age). Scale bar: 50 μ m (A and C) and 20 μ m (B and D); and the quantification of the number of NeuN-positive cells calculated for wild-type and CMVMJD135 mice in pontine nuclei (E). CMVMJD135 showed a trend towards decrease in the number of neurons, although not statistically significant.

4.2.1. Quantification of dopaminergic neurons in the substantia nigra.

Dopamine is a simple organic chemical in the catecholamine and phenethylamine families that plays a number of important roles in the brain. Inside the brain, dopamine functions as a neurotransmitter plays an important role in motor control and motivation. Dopaminergic neurons are neurons whose primary neurotransmitter is dopamine (Schultz, 2007). These neurons are confined to a few relatively small brain areas such as substantia nigra, however, they send projections to many other brain areas and exert powerful effects on their targets (Björklund and Dunnett, 2007). The degeneration of the neurons of the substantia nigra that send their axons to the corpus striatum results in a reduction in the release of the neurotransmitter dopamine within the corpus striatum. This leads to hypersensitivity of the dopamine receptors in the postsynaptic neurons in the striatum (Snell, 2000).

Tyrosine hydroxylase is the enzyme responsible for catalyzing the conversion of the amino acid L-tyrosine to L-3,4-dihydroxyphenylalanine (L-DOPA) (Kaufman, 1995). Since L-DOPA is the precursor for the neurotransmitter dopamine, we can assess dopaminergic neurons levels in substantia nigra by quantifying the tyrosine hydroxylase – immunopositive cells (Goti et al, 2004).

In this part of the work, we aimed to quantify the dopaminergic neurons in substantia nigra of CMVMJD135 and further compare the results with wild-type animals. For that, we performed immunohistochemistry anti-TH and quantified the TH-positive cells in substantia nigra of transgenic (n=4) and wild-type (n=3) animals at 93 weeks of age.

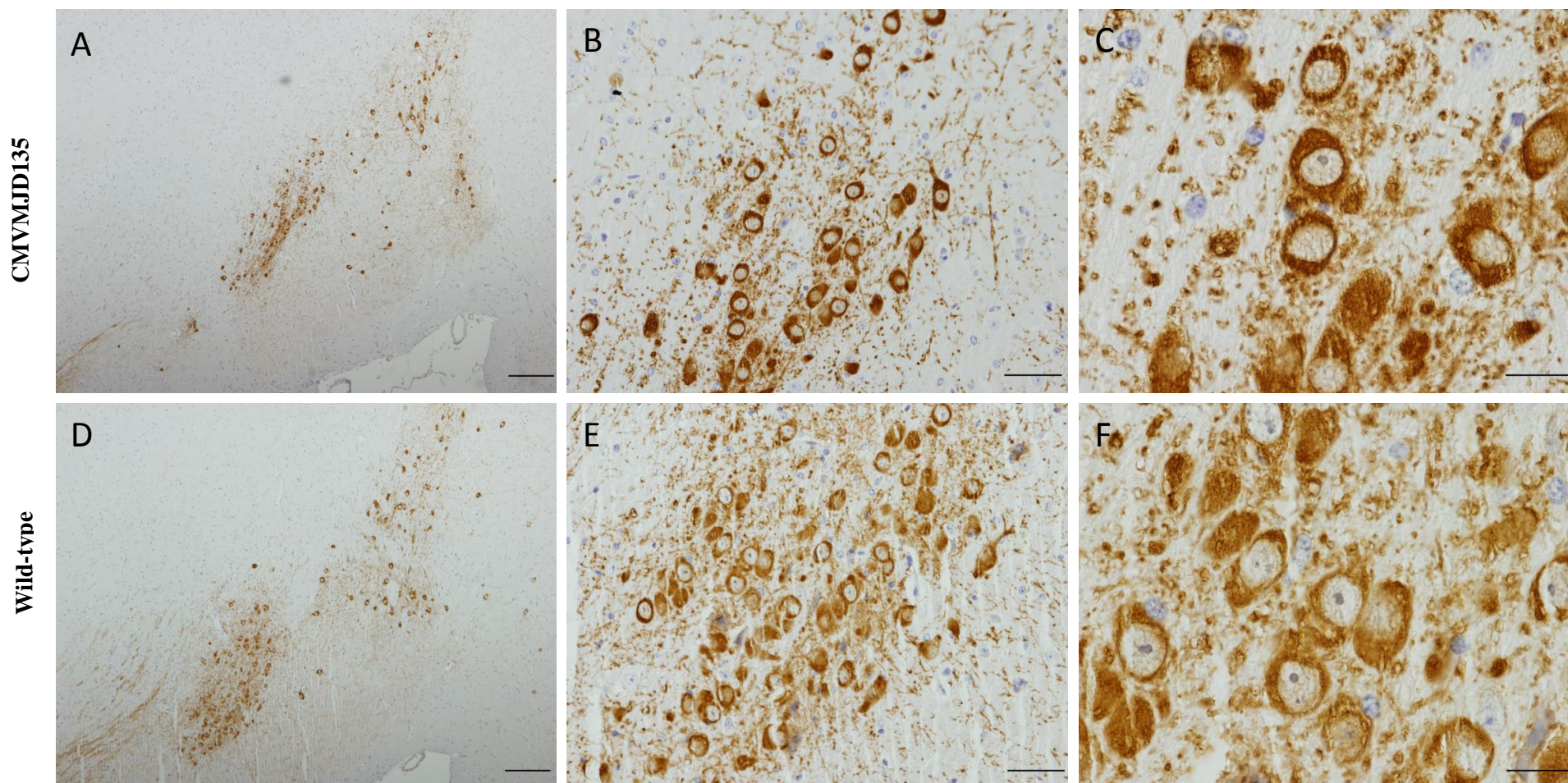


Figure 21. Tyrosine-hydroxylase (TH) immunostaining in substantia nigra in CMVMJD135 (A-C) and wild-type animals (D-F) at late stage of the disease (93 weeks of age). Scale bar: 200 μm (A and D) 50 μm (B and E) and 20 μm (C and F).

Our results demonstrate that CMVMJD135 transgenic mouse model have a statistically significant decrease of 28% of dopaminergic neurons in substantia nigra *pars compacta* when compared to wild-type animals ($p=0,0005$).

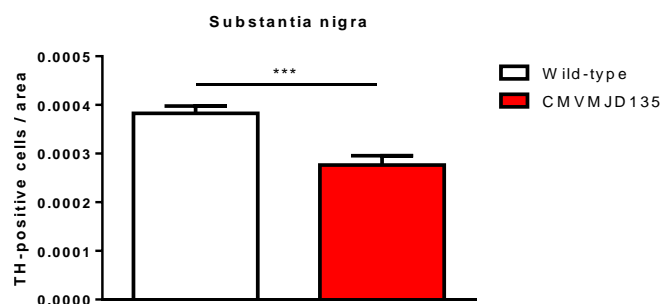


Figure 22. Number of TH-positive cells calculated for wild-type (σ n=3) and CMVMJD135 mice (σ n=4) in substantia nigra. Asterisks indicate significant differences between wild-type control and CMVMJD135 transgenic mice (** $p < 0.001$). CMVMJD135 showed a statistically significant decrease in the number of dopaminergic neurons (28%) in substantia nigra *pars compacta*.

4.3. Analysis of cerebellar layer thickness in CMVMJD135

The cerebellum is a region of the brain that plays an important role in motor control. Cerebellum contributes to coordination, precision, and accurate timing. It receives input from sensory systems of the spinal cord and from other parts of the brain, and integrates these inputs to fine tune motor activity (Fine et al, 2002). The cerebellum is located at the bottom of the brain and like the cerebral cortex, it is divided into two hemispheres. A set of large folds are conventionally used to divide the overall structure into ten smaller lobules layers. Because of its large number of tiny granule cells, the cerebellum contains more neurons than the rest of the brain put together (Snell, 2000).

There are three layers to the cerebellar cortex: the molecular, Purkinje, and granular. The innermost layer (granular) contains the cell bodies of two types of cells: the granule cells and the Golgi cells. Mossy fibers enter the granular layer from their main point of origin, the pontine nuclei. These fibers form excitatory synapses with the granule cells and the cells of the deep cerebellar nuclei. Golgi cells provide inhibitory feedback to granule cells, forming a synapse with them and projecting an axon into the molecular layer. The middle layer (Purkinje) contains only one type of cells— Purkinje cells. These cells are the primary integrative neurons of the cerebellar cortex and provide its sole output. Purkinje cell dendrites are large arbors with hundreds of spiny branches reaching up into the molecular layer. Purkinje neurons are GABAergic - meaning they have inhibitory synapses - with the neurons of the deep cerebellar and vestibular nuclei in the brainstem. The outermost layer (molecular) of the cerebellar cortex contains two types of inhibitory interneurons: the stellate and basket cells. It also contains the dendritic arbors of Purkinje neurons and parallel fiber tracts from the granule cells. Both stellate and basket cells form GABAergic synapses onto Purkinje cell dendrites (Voogd and Glickstein, 1998).

In this part of the work, we aimed to measure the thickness of molecular and granular layers of the cerebellum in CMVMJD135 and compare the values with wild-type animals. In order to do that, we analysed the thickness of these layers in transgenic (n=3) and wild-type (n=3) animals at 93 weeks of age.

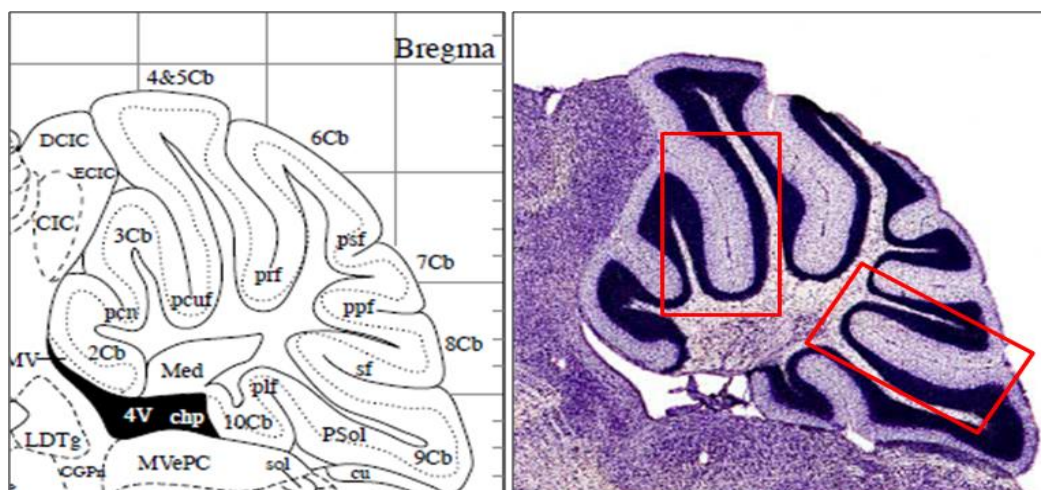


Figure 23. Low magnification micrograph of a sagittal section of cerebellum of the mouse stained with H&E and the corresponding atlas scheme used for the identification of the preculminate fissure (pcuf) and secondary fissure (sf).

Our results revealed a statistically significant ($p=0,044$) decrease of 10% of the thickness of the molecular layer in CMVMJD135 compared to the wild-type animals. However, no statistically significant differences were observed in the granular layer.

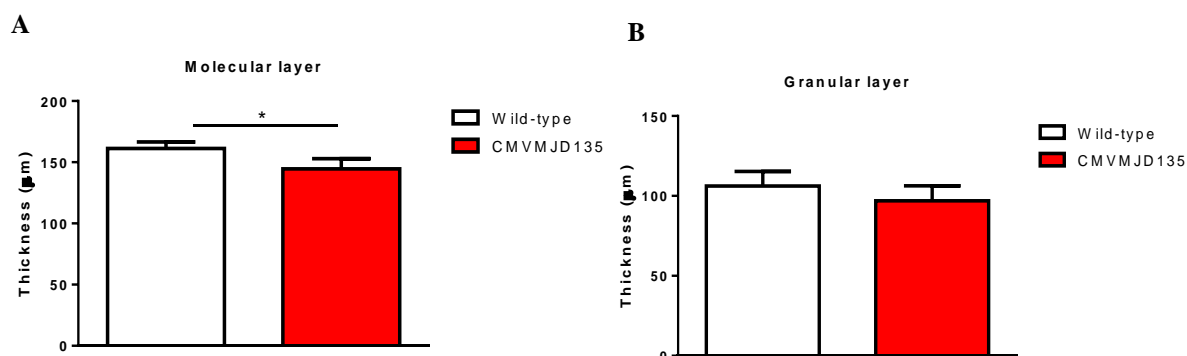


Figure 24. Measurements of molecular (A) and granular (B) layers of cerebellum calculated for wild-type (♂ $n=3$) and CMVMJD135 mice (♂ $n=3$). Asterisks indicate significant differences between wild-type control and CMVMJD135 transgenic mice ($*p<0.05$). CMVMJD135 showed a statistically significant decrease in the thickness of molecular layer. No differences were found in the granular layer.

5. DISCUSSION

5. DISCUSSION

Recently, our team generated a transgenic mouse model of MJD, CMVMJD135, that shows severe symptoms of the disease including balance deficits, motor uncoordination and weight loss, that appear and progress overtime. Taking into account that this mouse model presents severe symptoms of the disease we aimed to characterize the neuropathologic features, by performing stereological analysis in a selection of brain areas known to be affected in MJD patients, such as the substantia nigra in the midbrain (mesencephalon), the pontine nuclei in ventral pons, the locus coeruleus in the rostral pons (metencephalon) and dentate nuclei in the cerebellum. All of these regions play an important role in motor activity, which is compromised in MJD patients.

In this work, we performed stereological analyses in pontine nuclei and we found a loss of volume of 13% in our transgenic mice. Furthermore, we aim to clarify the basis of this volume reduction, so we quantified the total number of cells and we found a significant decrease of 12% in the cell number in the pontine nucleus. This reduction of cells is in the same proportion to that observed in the volume, so we could conclude that this reduction of volume was actually caused by a loss of cells. In order to better understand which type of cells was decreased, neurons or glial cells, we evaluated differentially, the number of each type of cells (astrocytes and neurons) in CMVMJD135 mice and compared the values with wild-type animals. We did not observe differences in the number of astrocytes; however, we were able to see a decrease, although not statistically significant, of the neurons number in pontine nuclei of CMVMJD135 mice. One possible explanation of this result owns to the fact that the reduction of volume and the reduction of the cell number are very similar suggesting that the cell density (number of cells/ area) trends to be the same independently of the dimension of the region. In order to confirm the trend towards a reduction in the total cell number, we should increase the number of animals in the study. Overall, the results observed in pontine nuclei are concordant with those found in MJD human patients, since mild to moderate neuronal loss is detected in the pontine nucleus of MJD patients (Yamada et al, 2008). Neuronal cell loss, although assessed by a non-specific quantification method, was previously reported in the pontine nuclei of MJD84.2 mouse model (Cemal et al, 2002). Signals of abnormal morphology of neurons were also described by the presence of hyperchromatic and shrunken scattered dark cells with

pyknotic nuclei and eosinophilic cytoplasm in pontine nuclei of several mouse models, including our CMVMJD135 transgenic mice (Cemal et al, 2002; Silva-Fernandes et al, 2010; Silva-Fernades et al, article submitted for publication).

The stereological analysis of locus coeruleus revealed a non-significant trend towards decrease in the volume as well as in the total number of cells. It is possible that CMVMJD135 do not have alterations in volume and cell number in this region, however to be more clear about this fact we should increase the number of animals used in the experiment, in order to reduce the individual variability observed in each group, which by itself generates an increased standard deviation that decreases the statistical significance of the results. On the other hand, this mouse model may have a slight, but not a severe atrophy of this region, or even a neuronal dysfunction that does not culminated in neuronal loss. Locus coeruleus is an affected brain region in MJD patients, who present loss of pigment and moderate neuronal loss of this region (Muñoz et al, 2002). However, so far no neuropathologic studies of the locus coeruleus have been described in the mouse models generated for MJD.

In order to evaluate the pathology of substantia nigra in our mouse model, we performed stereological analysis in this region. We did not observe any differences in terms of volume and total number of cells in substantia nigra of CMVMJD135 mice compared to wild-type animals. Pathological studies have demonstrated that MJD consists of a diffuse neurodegenerative process with a severe neuronal loss in substantia nigra (Riess et al, 2008). Our team previously observed increased reactive astrocytes in a phenomenon normally associated with neuronal demise in this region of the brain in the CMVMJD94 (Silva-Fernandes et al, 2010) as well as in CMVMJD135 (Silva-Fernandes et al, article submitted for publication). Thus, we decided to quantify the TH-positive neurons in the substantia nigra *pars compacta* of the CMVMJD135 mice. Our results showed a statistically significant decrease in the number of dopaminergic neurons (TH-positive neurons) in substantia nigra *pars compacta*. Intriguingly, and despite this TH-positive cells reduction, we could not observe differences in the volume and total cell number in substantia nigra. This might be explained by the subregion measured in this brain area. Substantia nigra is constituted by substantia nigra *pars compacta* and *pars reticulata*. In the stereological study we did not discriminate these two subdivisions. We could hypothesise that the substantia nigra *pars reticulata* might not be affected in CMVMJD135, and since it consists of a big part of the substantia nigra, we could be masking the results. To overcome this limitation, the stereological

measurements should be performed separately. The reduction of dopaminergic neurons observed is in concordance with that seen in human MJD patients whose neuropathological examination revealed a severe depigmentation of the substantia nigra (Rüb et al, 2005). Additionally, significant lower striatal DAT (dopamine transporter) density was also observed in patients brains (Braga-Neto et al, 2012). A recent study evaluated the correlation between substantia nigra hyperechogenicity with striatal DAT uptake in MJD patients and the authors raised the possibility that in MJD there may be iron deposition, neuromelanin content decrease, and microglial activation in the substantia nigra, leading to its hyperechogenicity, which can be associated with loss of presynaptic striatal dopaminergic terminals (Pedroso et al, 2013). Dopaminergic neurons are especially vulnerable to damage. The damage of these neurons in the substantia nigra results in a Parkinsonian syndrome that can be, although not often, found in human MJD patients, being characterized by tremor, hypokinesia, rigidity and postural instability (Rosenberg, 1992). Taking into account the mouse models of MJD, Goti and co-workers also found a 38% reduction of TH-positive neurons in the substantia nigra of MJD transgenic mice, using stereological techniques.

In this work we also analysed the volume and total cell number in dentate nuclei of the CMVMJD135 transgenic mice and further compare the results with wild-type control animals. Our results showed a statistically significant decrease of 37% of the volume of this region in CMVMJD135 mice. We did not find differences in the total number of cells, suggesting that the decreased volume cannot be explained by a decrease in the cell number but probably by the shrinkage of the cells. This phenomenon will be further studied by analysing the number of dendrites, their length and branching. Studies in MJD patients reveal that the main lesions in MJD are located in the spinocerebellar system and cerebellar dentate nuclei (Yamada et al, 2004). Previously, Cemal and co-workers reported neuronal loss in dentate nuclei of transgenic mouse model of MJD. This group also found increased GFAP staining with a few reactive astrocytes in dentate nuclei attributed to neuronal loss and indicative of gliosis (Cemal et al, 2002). In 2004, Goti and colleagues reported a stereologic study in dentate nuclei of a transgenic mouse model; they observed, although not statistically significant, a decrease in the volume of this region (Goti et al, 2004).

We also studied the cerebellar morphology in the CMVMJD135 mice. We analysed the thickness of molecular and granular layers of cerebellum in our transgenic mouse model at very late stage of the disease (93 weeks of age) and we found a

reduction of 10% of the molecular layer thickness. This finding is in accordance to what seen in MJD human patients at a late stage of the disease. The cerebellum has been suggested to be a major target of degenerative processes in MJD (Dürr et al, 1996). The cerebellar cortical neurons, however, are preserved in most cases and minimal loss of Purkinje cells are encountered in some patients. However, the cerebellar white matter is atrophic and shows myelin pallor due to degeneration of the pontocerebellar and spinocerebellar fibers (Yamada et al, 2008). Atrophy of molecular, Purkinje and granular cell layers is a morphological change seen in terminal clinical stages of cerebellar degeneration. Histological analysis performed in brains of some mouse models of MJD showed degeneration of all three layers of the cerebellum (Ikeda et al, 1996) and loss of Purkinje cells (Ikeda et al, 1996; Cemal et al 2002 and Bichelmeier et al, 2007). Reactive astrocytes were also reported in cerebellar white matter, which as referred before is an indicator of neuronal compromise (Cemal et al, 2002).

All together these results contribute to a more complete neuropathologic characterization of a new mouse model of MJD. These findings can contribute to define biomarkers of disease progression and achieve new therapy targets for MJD, in a mouse model that presents a severe phenotype of the disease with a neuronal loss pattern similar with human MJD patients observed in a late stage of the disease.

6. CONCLUSIONS

6. CONCLUSIONS

In this work we performed the neuropathological study of the CMVMJD135 mice and we observed:

At a late stage of the disease,

- A decrease of 13% of the total volume and 12% of the total cell number in pontine nuclei, and no differences in astrocyte and neurons number in this region.
- No differences in the volume and total number of cells in the locus coeruleus.
- A decrease of 37% of the total volume and no differences in the total cell number in the dentate nuclei.
- No differences in the total volume and total cell number in the substantia nigra and a reduction of 28% of dopaminergic neurons number in this region.
- A decrease of 10% in the thickness of the molecular layer of cerebellum and no differences in the granular layer thickness.

7. FUTURE PERSPECTIVES

7. FUTURE PERSPECTIVES

The CMVMJD135 transgenic mouse model shows an important overlap with neuropathologic features of MJD (Silva-Fernandes et al, submitted for publication). To further complement the study of the neuropathology of the CMVMJD135, we aim to:

- Analyse the morphology of dentate nuclei's neurons: number of dendrites, their length and branching as well as spine density once we observed a volume decrease in dentate nuclei that is not related with a decreased cell number.
- Quantify the number of glial cells in the substantia nigra of CMVMJD135 mice, since an increased number of these cells was found in a mouse model previously generated in our group for MJD, with milder disease.
- Evaluate the volume and total cell number of more CNS regions known to be involved in MJD, such as the Clarke's column in spinal cord, subthalamic nuclei in basal ganglia as well as facial nuclei in pons.
- Quantify the noradrenalin transporter (NAT) in the locus coeruleus of CMVMJD135 mice in order to assess the neuronal function of this region.
- Analyse the projections of substantia nigra to striatum (TH fibers) using the L-cycloid optical fractionator software.

8. REFERENCES

8. REFERENCES

Arrasate M, Mitra S, Schweitzer ES, Segal MR, Finkbeiner S. Inclusion body formation reduces levels of mutant huntingtin and the risk of neuronal death. *Nature* 431(7010):805-10, 2004.

Bauer PO, Nukina N. The pathogenic mechanisms of polyglutamine diseases and current therapeutic strategies. *J Neurochem* 110(6):1737-65, 2009.

Benarroch EE. The locus ceruleus norepinephrine system: functional organization and potential clinical significance. *Neurology* 73(20):1699-704, 2009.

Berridge CW, Waterhouse BD. The locus coeruleus-noradrenergic system: modulation of behavioral state and state dependent cognitive processes. *Brain Res Brain Res Rev* 42(1):33-84, 2003.

Bettencourt C, Lima M. Machado-Joseph Disease: from first descriptions to new perspectives. *Orphanet J Rare Dis* 6:35, 2011.

Bhatnagar SC. Neuroscience For the Study of Communicative Disorders 2nd Edition. Lippincott Williams & Wilkins, 2002.

Bichelmeier U, Schmidt T, Hübener J, Boy J, Rüttiger L, Häbig K, Poths S, Bonin M, Knipper M, Schmidt WJ, Wilbertz J, Wolburg H, Laccone F, Riess O. Nuclear localization of ataxin-3 is required for the manifestation of symptoms in SCA3: in vivo evidence. *J Neurosci* 27(28):7418-28, 2007.

Björklund A, Dunnett SB. Dopamine neuron systems in the brain: an update. *Trends Neurosci* 30(5):194-202, 2007.

Boy J, Schmidt T, Schumann U, Grasshoff U, Unser S, Holzmann C, Schmitt I, Karl T, Laccone F, Wolburg H, Ibrahim S, Riess O. A transgenic mouse model of spinocerebellar ataxia type 3 resembling late disease onset and gender-specific instability of CAG repeats. *Neurobiol Dis* 37(2):284-93, 2010.

Braga-Neto P, Felicio AC, Hoexter MQ, Pedroso JL, Dutra LA, Alessi H, Minetti T, Santos-Galduroz RF, da Rocha AJ, Garcia LA, Bertolucci PH, Bressan RA, Barsottini OG. Cognitive and olfactory deficits in Machado-Joseph disease: a dopamine transporter study. *Parkinsonism Relat Disord* 18(7):854-8, 2012.

Buhmann C, Bussopulos A, Oechsner M. Dopaminergic response in Parkinsonian phenotype of Machado-Joseph disease. *Mov Disord* 18(2):219-21, 2003.

Bürk K, Abele M, Fetter M, Dichgans J, Skalej M, Laccone F, Didierjean O, Brice A, Klockgether T. Autosomal dominant cerebellar ataxia type I clinical features and MRI in families with SCA1, SCA2 and SCA3. *Brain* 119 (Pt 5):1497-505, 1996.

Burnett B, Li F, Pittman RN. The polyglutamine neurodegenerative protein ataxin-3 binds polyubiquitylated proteins and has ubiquitin protease activity. *Hum Mol Genet* 12(23):3195-205, 2003.

Cemal CK, Carroll CJ, Lawrence L, Lowrie MB, Ruddle P, Al-Mahdawi S, King RH, Pook MA, Huxley C, Chamberlain S. YAC transgenic mice carrying pathological alleles of the MJD1 locus exhibit a mild and slow progressive cerebellar deficit. *Hum Mol Genet* 11(9):1075-94, 2002.

Chou AH, Yeh TH, Kuo YL, Kao YC, Jou MJ, Hsu CY, Tsai SR, Kakizuka A, Wang HL. Polyglutamine-expanded ataxin-3 activates mitochondrial apoptotic pathway by upregulating Bax and downregulating Bcl-xL. *Neurobiol Dis* 21(2):333-45, 2006.

Chou AH, Yeh TH, Ouyang P, Chen YL, Chen SY, Wang HL. Polyglutamine-expanded ataxin-3 causes cerebellar dysfunction of SCA3 transgenic mice by inducing transcriptional dysregulation. *Neurobiol Dis* 31(1):89-101, 2008.

Colomer Gould VF. Mouse models of Machado-Joseph disease and other polyglutamine spinocerebellar ataxias. *NeuroRx* 2(3):480-3, 2005.

- Colomer Gould VF. Mouse models of spinocerebellar ataxia type 3 (Machado-Joseph disease). *Neurotherapeutics* 9(2):285-96, 2012. Costa Mdo C, Paulson HL. Toward understanding Machado-Joseph disease. *Prog Neurobiol* 97(2):239-57, 2012.
- Coutinho P, Andrade C. Autosomal dominant system degeneration in Portuguese families of the Azores Islands. A new genetic disorder involving cerebellar, pyramidal, extrapyramidal and spinal cord motor functions. *Neurology* 28(7):703-9, 1978.
- D'Abreu A, França M Jr, Appenzeller S, Lopes-Cendes I, Cendes F. Axonal dysfunction in the deep white matter in Machado-Joseph disease. *J Neuroimaging* 19(1):9-12, 2009.
- Deniau JM, Hammond C, Riszk A, Feger J. Electrophysiological properties of identified output neurons of the rat substantia nigra (pars compacta and pars reticulata): evidences for the existence of branched neurons. *Exp Brain Res* 32(3):409-22, 1978.
- Dürr A, Stevanin G, Cancel G, Duyckaerts C, Abbas N, Didierjean O, Chneiweiss H, Benomar A, Lyon-Caen O, Julien J, Serdaru M, Penet C, Agid Y, Brice A. Spinocerebellar ataxia 3 and Machado-Joseph disease: clinical, molecular, and neuropathological features. *Ann Neurol* 39(4):490-9, 1996.
- Eichler L, Bellenberg B, Hahn HK, Köster O, Schöls L, Lukas C. Quantitative assessment of brain stem and cerebellar atrophy in spinocerebellar ataxia types 3 and 6: impact on clinical status. *AJNR Am J Neuroradiol* 32(5):890-7, 2011.
- Ekshyyan O, Aw TY. Apoptosis: a key in neurodegenerative disorders. *Curr Neurovasc Res* 1(4):355-71, 2004.
- Eng LF, Ghirnikar RS, Lee YL. Glial fibrillary acidic protein: GFAP-thirty-one years (1969-2000). *Neurochem Res* 25(9-10):1439-51, 2000.
- Evert BO, Vogt IR, Kindermann C, Ozimek L, de Vos RA, Brunt ER, Schmitt I, Klockgether T, Wüllner U. Inflammatory genes are upregulated in expanded ataxin-3-expressing cell lines and spinocerebellar ataxia type 3 brains. *J Neurosci* 21(15):5389-96, 2001.

Fine EJ, Ionita CC, Lohr L. The history of the development of the cerebellar examination. *Semin Neurol* 22(4):375-84, 2002.

Goti D, Katzen SM, Mez J, Kurtis N, Kiluk J, Ben-Haiem L, Jenkins NA, Copeland NG, Kakizuka A, Sharp AH, Ross CA, Mouton PR, Colomer V. A mutant ataxin-3 putative-cleavage fragment in brains of Machado-Joseph disease patients and transgenic mice is cytotoxic above a critical concentration. *J Neurosci* 24(45):10266-79, 2004.

Gundersen HJ, Jensen EB. The efficiency of systematic sampling in stereology and its prediction. *J Microsc* 147(Pt 3):229-63, 1987.

Gusella JF and MacDonald ME. Molecular genetics: unmasking polyglutamine triggers in neurodegenerative disease. *Nat Rev Neurosci* 1(2):109-15, 2000.

Herculano-Houzel S, Lent R. Isotropic fractionator: a simple, rapid method for the quantification of total cell and neuron numbers in the brain. *J Neurosci* 25(10):2518-21, 2005.

Horimoto Y, Matsumoto M, Yuasa H, Kojima A, Nokura K, Katada E, Yamamoto T, Yamamoto H, Mitake S. Brainstem in Machado-Joseph disease: atrophy or small size? *Eur J Neurol* 15(1):102-5, 2008.

Ichikawa Y, Goto J, Hattori M, et al. The genomic structure and expression of MJD, the Machado-Joseph disease gene. *J Hum Genet* 46(7):413-22, 2001.

Ikeda H, Yamaguchi M, Sugai S, Aze Y, Narumiya S, Kakizuka A. Expanded polyglutamine in the Machado-Joseph disease protein induces cell death in vitro and in vivo. *Nat Genet* 13(2):196-202, 1996.

Ishikawa K, Fujigasaki H, Saegusa H, et al. Abundant expression and cytoplasmic aggregations of [alpha]1A voltage-dependent calcium channel protein associated with neurodegeneration in spinocerebellar ataxia type 6. *Hum Mol Genet* 8(7):1185-93, 1999.

Jortner BS. The return of the dark neuron. A histological artifact complicating contemporary neurotoxicologic evaluation. *Neurotoxicology* (4):628-34, 2006.

Kanai K, Kuwabara S, Arai K, Sung JY, Ogawara K, Hattori T. Muscle cramp in Machado-Joseph disease: altered motor axonal excitability properties and mexiletine treatment. *Brain* 126(Pt 4):965-73, 2003.

Kaufman S. Tyrosine hydroxylase. *Adv Enzymol Relat Areas Mol Biol* 70:103-220, 1995.

Kawaguchi Y, Okamoto T, Taniwaki M, et al. CAG expansions in a novel gene for Machado-Joseph disease at chromosome 14q32.1. *Nat Genet* 8(3): 221-8, 1994.

Klockgether T, Schöls L, Abele M, Bürk K, Topka H, Andres F, Amoiridis G, Lüdtke R, Riess O, Laccone F, Dichgans J. Age related axonal neuropathy in spinocerebellar ataxia type 3/Machado-Joseph disease (SCA3/MJD). *J Neurol Neurosurg Psychiatry* 66(2):222-4, 1999.

Kumada S, Hayashi M, Mizuguchi M, Nakano I, Morimatsu Y, Oda M. Cerebellar degeneration in hereditary dentatorubral-pallidoluysian atrophy and Machado-Joseph disease. *Acta Neuropathol* 99(1):48-54, 2000.

La Spada AR, Wilson EM, Lubahn DB, Harding AE, Fischbeck KH. Androgen receptor gene mutations in X-linked spinal and bulbar muscular atrophy. *Nature* 352(6330):77-9, 1991.

Lukas C, Hahn HK, Bellenberg B, Hellwig K, Globas C, Schimrigk SK, Köster O, Schöls L. Spinal cord atrophy in spinocerebellar ataxia type 3 and 6: impact on clinical disability. *J Neurol* 255(8):1244-9, 2008.

Maciel P, Gaspar C, DeStefano AL et al. Correlation between CAG repeat length and clinical features in Machado-Joseph disease. *Am J Hum Genet* 57(1):54-61, 1995.

- Maciel P, Lopes-Cendes I, Kish S, Sequeiros J, Rouleau GA. Mosaicism of the CAG repeat in CNS tissue in relation to age at death in spinocerebellar ataxia type 1 and Machado-Joseph disease patients. *Am J Hum Genet* 60(4):993-6, 1997.
- Matos CA, de Macedo-Ribeiro S, Carvalho AL. Polyglutamine diseases: the special case of ataxin-3 and Machado-Joseph disease. *Prog Neurobiol* 95(1):26-48, 2011.
- Mehler MF, Purpura DP. Autism, fever, epigenetics and the locus coeruleus. *Brain Res Rev* 59(2):388-92, 2009.
- Muñoz E, Rey MJ, Milà M, Cardozo A, Ribalta T, Tolosa E, Ferrer I. Intranuclear inclusions, neuronal loss and CAG mosaicism in two patients with Machado-Joseph disease. *J Neurol Sci* 200(1-2):19-25, 2002.
- Nakano KK, Dawson DM, Spence A. Machado disease. A hereditary ataxia in Portuguese emigrants to Massachusetts. *Neurology* 22(1):49-55, 1972.
- Nicklas W, Baneux P, Boot R, Decelle T, Deeny AA, Fumanelli M, Illgen-Wilcke B. Recommendations for the health monitoring of rodent and rabbit colonies in breeding and experimental units. *Lab Anim* 36(1):20-42, 2002.
- Nishiyama K, Murayama S, Goto J, Watanabe M, Hashida H, Katayama S, Nomura Y, Nakamura S, Kanazawa I. Regional and cellular expression of the Machado-Joseph disease gene in brains of normal and affected individuals. *Ann Neurol* 40(5):776-81, 1996.
- Paxinos G, Franklin KBJ. *The Mouse Brain in Stereotaxic Coordinates* 2nd Edition. Academic Press, 2001.
- Paulson HL, Bonini NM, Roth KA. Polyglutamine disease and neuronal cell death. *Proc Natl Acad Sci U S A* 97(24):12957-8, 2000.
- Paulson HL. Dominantly inherited ataxias: lessons learned from Machado-Joseph disease/spinocerebellar ataxia type 3. *Semin Neurol* 27(2):133-42, 2007.

Paulson HL, Perez MK, Trotter Y, Trojanowski JQ, Subramony SH, Das SS, Vig P, Mandel JL, Fischbeck KH, Pittman RN. Intranuclear inclusions of expanded polyglutamine protein in spinocerebellar ataxia type 3. *Neuron* 19(2):333-44, 1997.

Pedroso JL, Bor-Seng-Shu E, Felício AC, Braga-Neto P, Hoexter MQ, Teixeira MJ, Bressan RA, Barsottini OG. Substantia nigra echogenicity is correlated with nigrostriatal impairment in Machado-Joseph disease. *Parkinsonism Relat Disord*, 2013.

Snell R. Clinical Neuroanatomy 7th Edition. Lippincott Williams & Wilkins, 2010.

Riess O, Rüb U, Pastore A, Bauer P, Schöls L. SCA3: neurological features, pathogenesis and animal models. *Cerebellum* 7(2):125-37, 2008.

Romanul FC, Fowler HL, Radvany J, Feldman RG, Feingold M. Azorean disease of the nervous system. *N Engl J Med* 296(26):1505-8, 1977.

Rosenberg RN, Nyhan WL, Bay C. Autosomal dominant striatonigral degeneration: a clinical, pathological, and biochemical study of a new genetic disorder. *Trans Am Neurol Assoc* 101:78-80, 1976.

Rosenberg RN. Machado-Joseph disease: an autosomal dominant motor system degeneration. *Mov Disord* 7(3):193-203, 1992.

Ross CA. When more is less: pathogenesis of glutamine repeat neurodegenerative diseases. *Neuron* 15(3):493-6, 1995.

Rüb U, Brunt ER, Deller T. New insights into the pathoanatomy of spinocerebellar ataxia type 3 (Machado-Joseph disease). *Curr Opin Neurol* 21(2):111-6, 2008.

Rüb U, de Vos RA, Brunt ER, Sebestény T, Schöls L, Auburger G, Bohl J, Ghebremedhin E, Gierga K, Seidel K, den Dunnen W, Heinsen H, Paulson H, Deller T. Spinocerebellar ataxia type 3 (SCA3): thalamic neurodegeneration occurs independently from thalamic ataxin-3 immunopositive neuronal intranuclear inclusions. *Brain Pathol* 16(3):218-27, 2006.

Rüb U, Gierga K, Brunt ER, de Vos RA, Bauer M, Schöls L, Bürk K, Auburger G, Bohl J, Schultz C, Vuksic M, Burbach GJ, Braak H, Deller T. Spinocerebellar ataxias types 2 and 3: degeneration of the pre-cerebellar nuclei isolates the three phylogenetically defined regions of the cerebellum. *J Neural Transm* 112(11):1523-45, 2005.

Schöls L, Bauer P, Schmidt T, Schulte T, Riess O. Autosomal dominant cerebellar ataxias: clinical features, genetics, and pathogenesis. *Lancet Neurol* 3(5):291-304, 2004.

Seidel K, den Dunnen WF, Schultz C, Paulson H, Frank S, de Vos RA, Brunt ER, Deller T, Kampinga HH, Rüb U. Axonal inclusions in spinocerebellar ataxia type 3. *Acta Neuropathol* 120(4):449-60, 2010.

Seidel K, Siswanto S, Brunt ER, den Dunnen W, Korf HW, Rüb U. Brain pathology of spinocerebellar ataxias. *Acta Neuropathol* 124(1):1-21, 2012.

Silva-Fernandes A, Costa Mdo C, Duarte-Silva S, Oliveira P, Botelho CM, Martins L, Mariz JA, Ferreira T, Ribeiro F, Correia-Neves M, Costa C, Maciel P. Motor uncoordination and neuropathology in a transgenic mouse model of Machado-Joseph disease lacking intranuclear inclusions and ataxin-3 cleavage products. *Neurobiol Dis* 40(1):163-76, 2010.

Silva-Fernandes A, Duarte-Silva S, Neves-Carvalho A, Amorim AM, Soares-Cunha C, Oliveira P, Thirstrup K, Teixeira-Castro A, Maciel P. Chronic treatment with 17-DMAG improves balance and coordination in a new mouse model of Machado-Joseph disease, *submitted for publication*.

Saudou F, Finkbeiner S, Devys D, Greenberg ME, Huntington acts in the nucleus to induce apoptosis but death does not correlate with formation of intranuclear inclusions. *Cell* 95(1):55-66, 1998.

Schultz W. Multiple dopamine functions at different time courses. *Annu Rev Neurosci* 30:259-88, 2007.

Sequeiros J, Coutinho P. Epidemiology and clinical aspects of Machado-Joseph disease. *Adv Neurol* 61:139-53, 1993.

Sterio DC. The unbiased estimation of number and sizes of arbitrary particles using the disector. *J Microsc* 134(Pt 2):127-36, 1984.

Sultan F, Hamodeh S, Baizer JS. The human dentate nucleus: a complex shape untangled. *Neuroscience* 167(4):965-8, 2010.

Takahashi T, Katada S, Onodera O. Polyglutamine diseases: where does toxicity come from? what is toxicity? where are we going?. *J Mol Cell Biol* 2(4):180-91, 2010.

Takiyama Y, Nishizawa M, Tanaka H, et al. Nat Genet. The gene for Machado-Joseph disease maps to human chromosome 14q. *Nat Genet* 4(3):300-4. 1993.

Taniwaki T, Sakai T, Kobayashi T, Kuwabara Y, Otsuka M, Ichiya Y, Masuda K, Goto I. Positron emission tomography (PET) in Machado-Joseph disease. *J Neurol Sci* 145(1):63-7, 1997.

Trottier Y, Cancel G, An-Gourfinkel I, Lutz Y, Weber C, Brice A, Hirsch E, Mandel JL. Heterogeneous intracellular localization and expression of ataxin-3. *Neurobiol Dis* 5(5):335-47, 1998.

Voogd J, Glickstein M. The anatomy of the cerebellum. *Trends Neurosci* 21(9):370-5, 1998.

West MJ, New stereological methods for counting neurons. *Neurobiol Aging* 14(4): 275-85, 1993.

West MJ, Slomianka L, Gundersen HJ. Unbiased stereological estimation of the total number of neurons in the subdivisions of the rat hippocampus using the optical fractionator. *Anat Rec* 231(4):482-97, 1991.

Williams LC, Hegde MR, Herrera G, Stapleton PM, Love DR. Comparative semi-automated analysis of (CAG) repeats in the Huntington disease gene: use of internal standards. *Mol Cell Probes* 13(4):283-9, 1999.

Woods BT, Schaumburg HH. Nigro-spino-dentatal degeneration with nuclear ophthalmoplegia. A unique and partially treatable clinico-pathological entity. *J Neurol Sci* 7(2):149-66, 1972.

Yamada M, Sato T, Tsuji S, Takahashi H. CAG repeat disorder models and human neuropathology: similarities and differences. *Acta Neuropathol* 115(1):71-86, 2008.

Yamada M, Tan CF, Inenaga C, Tsuji S, Takahashi H. Sharing of polyglutamine localization by the neuronal nucleus and cytoplasm in CAG-repeat diseases. *Neuropathol Appl Neurobiol* 30(6):665-75, 2004.

Wüllner U, Reimold M, Abele M, Bürk K, Minnerop M, Dohmen BM, Machulla HJ, Bares R, Klockgether T. Dopamine transporter positron emission tomography in spinocerebellar ataxias type 1, 2, 3, and 6. *Arch Neurol* 62(8):1280-5, 2005.

Zoghbi HY, Orr HT. Glutamine repeats and neurodegeneration. *Annu Rev Neurosci* 23:217-47, 2000.